

# Finding anomalous periodic time series

## An application to catalogs of periodic variable stars

Umaa Rebbapragada · Pavlos Protopapas ·  
Carla E. Brodley · Charles Alcock

Received: 20 March 2007 / Revised: 17 November 2008 / Accepted: 21 November 2008 /  
Published online: 31 December 2008  
Springer Science+Business Media, LLC 2008

**Abstract** Catalogs of periodic variable stars contain large numbers of periodic light-curves (photometric time series data from the astrophysics domain). Separating anomalous objects from well-known classes is an important step towards the discovery of new classes of astronomical objects. Most anomaly detection methods for time series data assume either a single continuous time series or a set of time series whose periods are aligned. Light-curve data precludes the use of these methods as the periods of any given pair of light-curves may be out of sync. One may use an existing anomaly detection method if, prior to similarity calculation, one performs the costly act of aligning two light-curves, an operation that scales poorly to massive data sets. This paper presents PCAD, an unsupervised anomaly detection method for large sets of unsynchronized periodic time-series data, that outputs a ranked list of both global and local anomalies. It calculates its anomaly score for each light-curve in relation to a set of centroids produced by a modified k-means clustering algorithm. Our method is able to scale to large data sets through the use of sampling. We validate our method on both light-curve data and other time series data sets. We demonstrate its effectiveness at finding known anomalies, and discuss the effect of sample size and number of centroids on our results. We compare our method to naive solutions and existing time series anomaly detection

---

Editor: Tow Fawcett.

U. Rebbapragada (✉) · C.E. Brodley  
Department of Computer Science, Tufts University, 161 College Ave., Medford, MA 02155, USA  
e-mail: [urebbapr@cs.tufts.edu](mailto:urebbapr@cs.tufts.edu)

C.E. Brodley  
e-mail: [brodley@cs.tufts.edu](mailto:brodley@cs.tufts.edu)

P. Protopapas · C. Alcock  
Harvard-Smithsonian Center for Astrophysics, 60 Garden Street, Cambridge, MA 02138, USA

P. Protopapas  
e-mail: [pprotopapas@cfa.harvard.edu](mailto:pprotopapas@cfa.harvard.edu)

C. Alcock  
e-mail: [calcock@cfa.harvard.edu](mailto:calcock@cfa.harvard.edu)

P. Protopapas  
Initiative in Innovative Computing, Harvard University, 60 Oxford Street, Cambridge, MA 02138, USA

methods for unphased data, and show that PCAD's reported anomalies are comparable to or better than all other methods. Finally, astrophysicists on our team have verified that PCAD finds true anomalies that might be indicative of novel astrophysical phenomena.

**Keywords** Anomaly detection · Time series data

## 1 Introduction

Quasars (Schmidt 1963), radio pulsars (Hewish et al. 1968), and cosmic gamma-ray bursts (Klebesadel et al. 1973) were all discovered by alert scientists who, while examining data for a primary purpose, encountered aberrant phenomena whose further study led to these legendary discoveries. Such discoveries were possible in an era when scientists had a close connection with their data. The advent of massive data sets renders unexpected discoveries through manual inspection improbable if not impossible. Fortunately, automated anomaly detection programs may resurrect this mode of discovery and identify atypical phenomena indicative of novel astronomical objects.

Our research applies anomaly detection to photometric time series data, called *light-curve* data. Our specific application is to find anomalies in sets of light-curves of periodic variable stars. Most stars, like our own Sun, are of almost constant luminosity, whereas variable stars undergo significant variations. There are over 350,000 cataloged variable stars with more being discovered. The 2003 General Catalogue of Variable Stars (Samus' et al. 2003) lists known and suspected variable stars in our own galaxy, as well as 10,000 in other galaxies. For *periodic* variable stars, the period of the star can be established. Common types of periodic variable stars include Cepheid, Eclipsing Binaries and RR Lyrae, details of which can be found in Petit (1987), Sterken and Jaschek (1996), Richter et al. (1985).

The study of periodic variable stars is of great importance to astronomy. For example, the study of Cepheids yielded the most valuable method for determining the Hubble constant, and the study of binary stars enabled the discovery of a star's true mass. Finding a new class or subclass of variable stars will be of tremendous value.

Figure 1 shows a typical light-curve from each star class before and after we perform our pre-processing techniques (described in Sect. 6). The  $y$ -axis measures the magnitude of brightness of the star.<sup>1</sup> Magnitude is inversely proportional to the brightness of the observation, thus, the  $y$ -axis is plotted with descending values. The  $x$ -axis measures folded time. A folded light-curve is a light-curve where all periods are mapped onto a single period, which is why there may be multiple points on the  $y$ -axis for a single time point. We describe light-curves and the process of folding in more detail in Sect. 6.

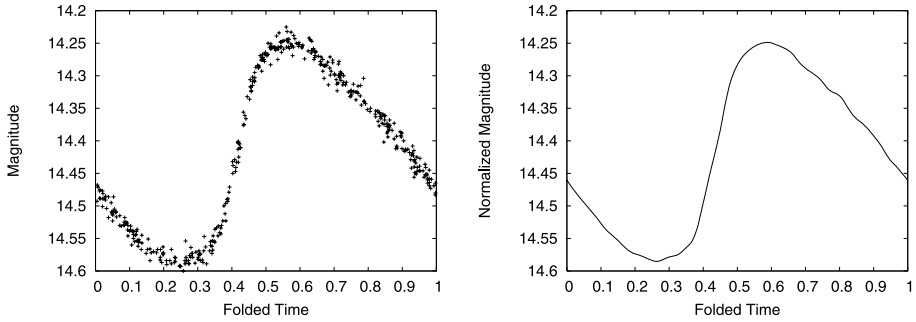
Our research is motivated by the challenges inherent to performing anomaly detection on large sets of periodic variable light-curves. Several of these challenges are common to many time series data sets. There are a large number of time-points in each light-curve (high dimensionality), low signal-to-noise ratio, and voluminous amounts of data. Indeed, new surveys, such as the Panoramic Survey Telescope and Rapid Response System (Pan-STARRS), have the capacity to produce light-curves for billions of stars.<sup>2</sup> Any technique developed for light-curves must scale to very large data sets.

A unique challenge of working with light-curve data is that the periods of the light-curves are not synchronized because each is generated by a different source (star). To understand

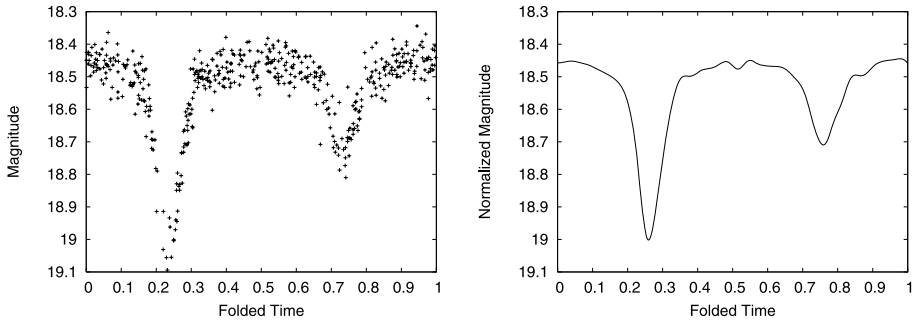
---

<sup>1</sup>Magnitude refers to the logarithmic measure of the brightness of an object.

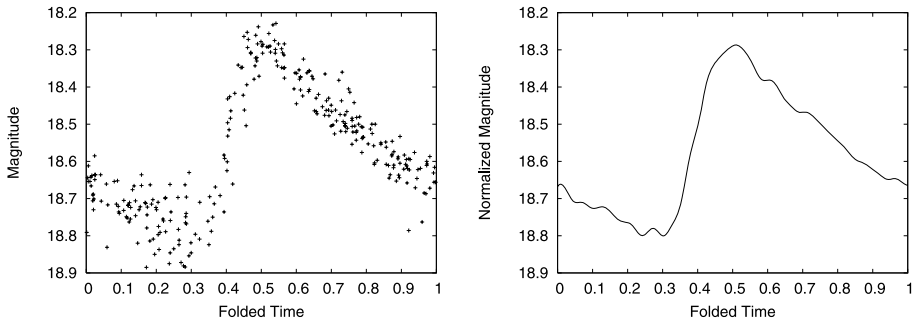
<sup>2</sup><http://pan-starrs.ifa.hawaii.edu/public/>. Panoramic survey telescope and rapid response system.



(a) Cepheid. OGLE-LMC\_SC4-53463. Period 5.4 days.



(b) Eclipsing Binary. OGLE052209.11-694441.9. Period 7.7 days.



(c) RR Lyrae. OGLE053520.04-703554.2. Period 0.34 days.

**Fig. 1** Examples of typical folded light-curves before (*left*) and after (*right*) pre-processing. For purposes of visual presentation, we align the maxima of each light-curve at approximately 0.25. This is also known as universal phasing, which is discussed in Sect. 3

why phasing poses such a challenge for anomaly detection in this domain, consider Fig. 2, which illustrates how two similar light-curves may appear dissimilar under a similarity measure like Euclidean distance if a phase adjustment is not performed. The top panel shows two similar light-curves whose phases are not synchronized. The middle panel shows the square of the correlation plotted as a function of the phase adjustment. The maximum similarity occurs at a phase shift of approximately 0.3. The bottom panel shows the two light-curves after

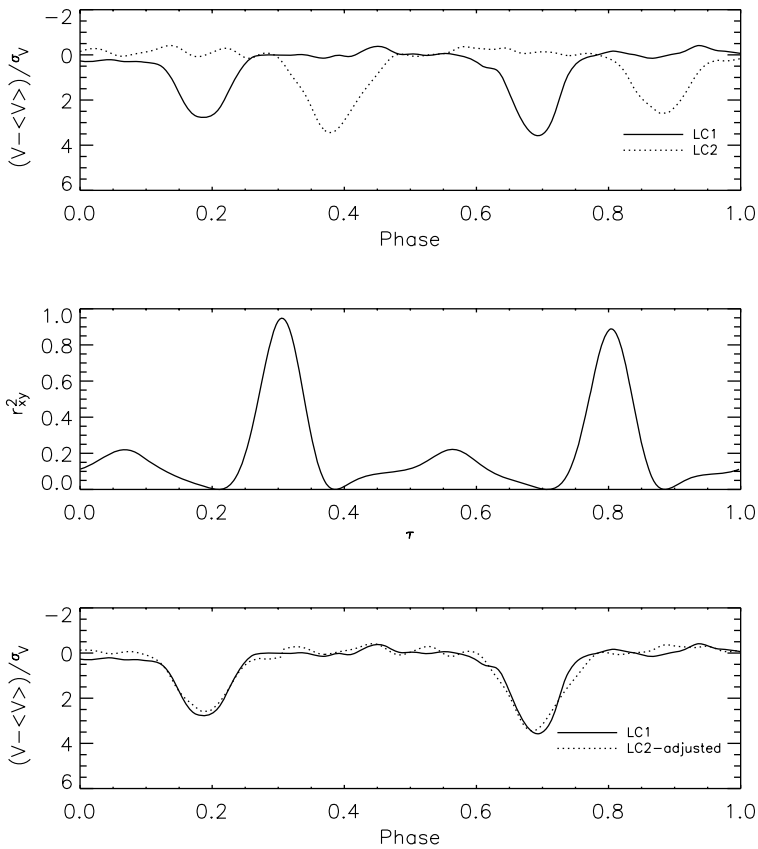


**Fig. 2** The *top panel* shows two light-curves that are similar but whose phases are not synchronized. The *middle panel* plots the square of the correlation as a function of the phase adjustment and shows that the global maximum occurs at a phase shift of approximately 0.3. The *bottom panel* shows the light-curves after shifting the *dotted curve* to the right by this amount

the dotted light-curve is shifted by this amount. We define the optimal phase shift between two light-curves as the shift that yields the maximum similarity value.

This phasing problem presents a challenge to both general anomaly detection techniques, and those developed specifically for time series. A general anomaly detection method, even with a metric that works for unphased data, may not work out of the box. With regard to time series anomaly detection techniques, our task of finding anomalies in  $n$  distinct time series differs from most work which assumes a single contiguous time series (not necessarily periodic) in which anomalous sub-regions are sought.

PCAD is our solution to the problem of anomaly detection on large sets of unsynchronized periodic time series. The heart of PCAD is a modified k-means clustering algorithm, called Phased K-means (Pk-means), that runs on a sampling of the data. Pk-means differs from k-means in that it re-phases each time series prior to similarity calculation and updates centroids from these rephased curves. Because Pk-means is a modification of k-means, we provide a proof that Pk-means does not break k-means's convergence properties.

The Pk-means subroutine runs offline on a sampling of the data. The use of sampling enables PCAD to scale to large data sets. The online portion of PCAD is the calculation

of the anomaly score for each time series from the set of centroids produced offline by Pk-means. This operation is linear in the size of the data set.

Another advantage of PCAD is its flexibility to discover two types of anomalies: local and global. We define the terms local and global anomaly and provide scoring methods for both. Once each time series is assigned an anomaly score, PCAD ranks the time series accordingly and outputs the top  $m$  for review. To our knowledge, PCAD is the only anomaly detection method developed specifically for unsynchronized time series data that can output both global and local anomalies.

Our paper presents empirical evidence on four data sets that PCAD effectively finds known anomalies and produces a better ranking of anomalies when compared to naive solutions and other state-of-the-art anomaly detection methods for time series. We discuss the effect of sample size and the parameter  $k$  (used by Pk-means) on the anomaly detection results, and show experimental results on light-curve data with an unknown number of anomalies. Our paper concludes with an astrophysicists's discussion of the significance of the anomalies found by PCAD.

## 2 Related work

PCAD is specifically developed to solve the problem of anomaly detection on unsynchronized periodic time series data. Because there are few other methods with this purpose, we organize our related work into three categories. First, we briefly review general anomaly detection methods for local and global outliers. We then provide an in-depth review of anomaly detection methods for time series data. We conclude with a discussion of time series methods designed for unsynchronized data.

### 2.1 Anomaly detection

Anomaly, or outlier, detection is a research area in both statistics and data mining. Statistical approaches focus on finding outliers with respect to a particular statistical model or distribution, and employ hypothesis testing for the discovery of outliers (Hawkins 1980; Barnett and Lewis 1994). Knorr and Ng define *distance-based outliers* (Knorr and Ng 1998) as a point that is greater than distance  $D$  away from at least  $p$  percent of the data set. The authors show that one can choose  $D$  and  $p$  to be compatible with statistical definitions of outliers. An advantage of the distance-based outlier definition is that it sidesteps the need to assume a parametric form for the data. However, one must know or search for the appropriate values of  $D$  and  $p$ . Other variants of the distance-based outlier definition include the distance of a point to its  $k$ -th nearest neighbor (Ramaswamy et al. 2000), or the sum of the distances to its  $k$ -nearest neighbors (Angiulli and Pizzuti 2002).

The methods presented by Knorr and Ng include a simple brute-force comparison of examples that avoids the use of indexing structures and is  $O(n^2)$ , and a faster cell-based method that is  $O(n)$  but exponential in the number of features. Subsequent approaches improve on computational efficiency or scale to high-dimensional data sets. Ramaswamy et al.'s method improves efficiency by partitioning the data into disjoint subsets and pruning calculations among subsets containing no outliers (Ramaswamy et al. 2000). Bay and Schwabacher employ pruning and randomization to achieve near-linear time performance (Bay and Schwabacher 2003). Wu and Jermaine find each example's  $k$ -nearest neighbors with respect to a random sample, rather than the entire data set (Wu and Jermaine 2006).

The distance-based outlier definition does not correctly identify outliers in mixed variance data. Breunig et al. introduced the local outlier factor (LOF) as a solution (Breunig et

al. 2000). Rather than setting a hard threshold  $D$ , LOF considers the density of an example's neighborhood to calculate an outlier score. Thus, density-based outlier detection algorithms are able to discover *local* outliers, or points that are anomalous with respect to their nearest neighbors or assigned cluster, as opposed to *global* outliers, points that are anomalous with respect to the entire data set. Other density-based outlier detection research improves the computational efficiency of LOF by summarizing the data (Jin et al. 2001) and indexing (Ren et al. 2004).

Both the distance- and density-based outlier definitions do not work well in high dimensions due to the curse of dimensionality. Solutions to outlier detection on high dimensional data include feature transformation (Angiulli and Pizzuti 2002; Yu et al. 2004), subspace projections (Aggarwal and Yu 2001; Lazarevic and Kumar 2005) and sampling (Kollios et al. 2003; Wu and Jermaine 2006).

In theory, the methods above can generalize to any type of data, including time series data, if one were able to apply an appropriate distance metric. In Sect. 3, we discuss why these methods may not be appropriate for large sets of unsynchronized time series data. Moreover, all of the methods described above output either distance-based global anomalies or density-based local anomalies. In contrast, PCAD has the flexibility to find both distance-based local or global anomalies.

## 2.2 Time series anomaly detection

Methods for time series anomaly detection operate either on a single time series or on a time series database. The goal of anomaly detection on a single time series is to find an anomalous subregion. The goal of anomaly detection on a time series database is to find an anomalous example. In some cases, a single time series is converted to a time series database through the use of a sliding window.

Many time series methods supply their own definitions of anomaly, rather than use the distance- and density-based definitions above. Some define anomalies with respect to a *reference data set* of "normal" time series. The anomalies discovered in this context are global anomalies. Other techniques use only the input data set, which contains both normal examples and the unknown anomalies. Depending on the amount of data used to compute their models, these techniques discover either global or local anomalies. For each technique, we comment on whether the method makes use of a reference set. For techniques using only the input data, we comment on whether global or local anomalies are sought.

In order to find an anomalous subregion within a single time series, one may slide a window across the data either incrementally (Dasgupta and Forrest 1996; Keogh et al. 2002; Ma and Perkins 2003; Wei et al. 2005) or in discrete steps according to a known period (Yang et al. 2001, 2004). Dasgupta and Forrest (1996), and Keogh et al.'s (2002) methods use sliding windows and discretization on a single continuous time series, and define anomalies with respect to a reference time series. They convert both their reference and input time series into two time series databases by sliding a window of user-specified length and discretizing the values in the window into a string. In Forrest and Dasgupta's work, a set of detectors is trained on the reference set such that no detector will match any member of that reference set. The detectors are then applied to the input set. Any example that signals an alarm is an anomaly. Keogh et al. encodes the set of discretized strings from both the reference and input sets in suffix trees. The surprise score of each string in the input set is calculated by comparing its number of occurrences in the input set versus its expected number of occurrences. These expectations are calculated using a Markov model built from the reference set. If the actual number of occurrences differs from the expected number of occurrences by more than a user-specified threshold, the string is flagged as an anomaly.

Wei et al.'s method finds local anomalies without the aid of a reference set (Wei et al. 2005). The method discretizes the time series using the SAX algorithm (Lin et al. 2003) and then slides two windows, called a "lead" and "lag" window, both of user-specified length, across the data. The lead window contains the sequence to be labeled as normal or anomalous. The lag window data acts a reference set. The lead window's anomaly score is the distance between the lead and lag windows, where the distance metric calculates the difference in frequency between all possible SAX subwords of a given size. A drawback of this method is that a small cluster of anomalies in the lag window might cause an anomalous pattern to be flagged as normal.

Discretization is often used to reduce the computation time of operations on the sliding window. In the three methods described above, comparisons are done in a discretized space. A criticism of this approach is that discretization may hurt the anomaly detection process because too few symbols may overly smooth the data, obfuscating some anomalies. The degree of smoothing at which this happens is dataset specific and remains an open area of research.

Ma and Perkins's method, also for a single continuous time series, uses a sliding window of user-specified length but does not employ discretization (Ma and Perkins 2003). Rather, it uses support vector regression to model all previously seen subsequences. For an incoming time point, the sliding window shifts forward one point and the newest input subsequence is evaluated with respect to the current model. If the input sequence differs from the model by more than a user-specified tolerance, the sequence is anomalous. The model is continually retrained with each incoming time point. Because the computation time of the method increases with each incoming data point, the authors propose dropping older samples in order to keep the size of the training set constant. A drawback of their approach is that it requires the user to specify six parameters, including sliding window size and kernel function. The authors acknowledge having no guidance for finding the optimal set of parameter values and declare this to be an area of future work.

Unlike methods that seek anomalies of a pre-specified length, Shahabi et al.'s method looks for anomalies at varying levels of granularity (i.e., day, month, year) (Shahabi et al. 2000). The authors develop a tree structure called TSA-Tree that contains pre-computed trend and anomaly information in each node. The tree grows to depth  $k$  where granularity decreases as the tree-depth increases. The authors use feature extraction (wavelet filters) to capture trend and surprise information at each granularity. However, the types of surprises are limited to "sudden changes" in the data that are captured by "local maximums".

Yang et al.'s InfoMiner technique detects "surprising" patterns on periodic event sequence data (Yang et al. 2001, 2004). Thus, the data are already discretized, and the known period allows the authors to treat a single continuous time series as a set of smaller one-period time series. InfoMiner detects global anomalies by calculating information gain on each sequence, and labeling that sequence as anomalous if its information gain exceeds a certain threshold. Because this technique is for event sequence data, the use of this program on real-valued time series data would require discretization of the data set, and comparisons in discretized space.

The next two methods are developed for time series databases. Salvador et al.'s method creates a finite automaton trained on a reference set of time series data (Salvador et al. 2004). An input time series is anomalous if it does not conform to the model, thus ending at an anomalous state. The state transition logic for the automaton is determined by a three step process. First, each reference time series is segmented using a novel clustering algorithm called Gecko that determines the appropriate number of segments. Second, the slope is extracted from each segment and then mapped to rules that are, in the third step, converted

into state-transition logic. Time does not figure into the features that are used to map segments to states. This meets the specific needs of their application (faulty valve detection), but would not work for a domain in which the relationship of the signal to time must be preserved.

Jagadish et al. find “deviants” in a time series database by modeling the time series with a set of minimum-bounding rectangles or “histograms” (Jagadish et al. 1999). Dynamic programming is used to find the optimal number of rectangles and rectangle-width. The  $k$  most deviant time points are first identified. These are points whose removal best improves the fit between the histogram and the original time series. After identifying deviant points, the method then identifies anomalous subregions as those having a number of deviants that exceeds a user threshold. Jagadish et al.’s technique, which finds global anomalies, is quadratic in the length of the time series and therefore too slow for light-curve and other voluminous time series data.

### 2.3 Time series methods for unphased data

The majority of time series methods that tackle the problem of unsynchronized data have the goal of time series clustering (Bar-Joseph et al. 2002; Chudova et al. 2003; Gaffney and Smyth 2004). These methods are applied to a diverse set of applications including the tracking of cyclone trajectories (Chudova et al. 2003), gene expression (Gaffney and Smyth 2004; Chudova et al. 2003; Bar-Joseph et al. 2002), and botany (Listgarten et al. 2006). Clearly, unsynchronized time series data sets exist in domains outside of astrophysics.

Of the methods cited above, only Gaffney and Smyth (2004) and Chudova et al. (2003) integrate data synchronization into their clustering methods. Both use the EM algorithm (Dempster et al. 1977) to estimate cluster membership as well as the amount of horizontal shift that occurs in each time series. Gaffney and Smyth develop a fully Bayesian generative model in “curve space”, which means they represent the curves using a regression mixture model. Thus, the time series need not be of uniform length. Their joint clustering-alignment model also assumes a normal regression model for the cluster labels, and Gaussian priors on the (hidden) transformation variables, where transformations include shifting and scaling on both the time axis and in measurement space. Chudova et al. (2003) develop a generative model that assumes uniformly spaced time points, but also multi-dimensional curves. Their model is formed in the time domain where the distribution of each curve minus its offset in both time and measurement space is assumed to be multivariate Gaussian with a diagonal covariance matrix. The authors employ conjugate priors on the model parameters, and use Gibbs sampling to obtain point estimates of both parameters and hyperparameters. Note that the goal of both methods is to produce the best clustering model. In contrast, PCAD uses a much simpler clustering method (that makes no parametric assumptions) for the purpose of anomaly detection. Their results show that applying EM to these Bayesian generative models produces good clustering results on unsynchronized data. However, for our application, these computationally intensive methods are unnecessary for the purpose of anomaly detection.

We discuss in detail the methods that do anomaly detection on unsynchronized time series data. Chan and Mahoney’s technique creates a model of minimum-bounding rectangles from a reference set of  $n$  normal time series (Chan and Mahoney 2005; Mahoney and Chan 2005). Before computing this model, each time point in each time series is mapped to a three-dimensional vector where the attributes are the smoothed time point plus its smoothed first and second derivatives. A box model is created for each reference time series using a greedy algorithm that finds  $x$  boxes that minimize the volume over the three-dimensional



feature space. Given the  $n$  separate box models, the two closest boxes across the different time series are repeatedly merged until only  $k$  remain. An anomaly score is calculated for an input time series by transforming the series into the three-dimensional feature space and summing each point's distance to the nearest box in the model. Because this algorithm trains a model on multiple time series, the authors also encounter the phasing issue, which they acknowledge with the statement: “two time series with corresponding behavior might not begin and end at the same time in the time series.” The authors handle phasing by allowing any two boxes to merge, regardless of their order in the original time series. It is our opinion that this “order-independent” algorithm may be too lenient, because it is possible to completely rearrange a time-series with this method. In contrast, the phase adjustment done by PCAD shifts a time series horizontally but otherwise respects the order of points. Also, Chan and Mahoney's method requires a reference set containing only typical examples from which a model of normality is calculated. PCAD does not use a reference set because a comprehensive set of typical examples is a luxury our domain experts may not be able to provide.

Wei et al.'s rotation-invariant discord discovery technique, which we refer to as RI-DISCORD (Wei et al. 2006), is an anomaly detection methods that discovers global anomalies or *discords* in shape data. Discords, whose definition is reminiscent of the distance-based outlier definition, are the  $m$  most anomalous time series (or subregions if the input is a single time series) with the farthest nearest neighbors (Keogh et al. 2005). The definition can also be extended to find the top  $m$  examples with the farthest distance to their  $k$ -nearest neighbors. RI-DISCORD takes a database of shape data as input, each of which is converted to a time series. In order to ensure that different rotations of the same shape matches another, Wei et al. use a rotation-invariant Euclidean distance measure that searches over all possible rotations of the time series and outputs the minimum distance calculated.

The  $O(n^2)$  brute-force version RI-DISCORD is identical to the brute-force version of Keogh et. al's discord detection method called HOT SAX (Keogh et al. 2005). The only difference is the use of the rotation-invariant distance measure in RI-DISCORD. Both have faster versions that use heuristics to order the inner and outer loops of the search in a way that ensures maximal pruning of distance calculations, but they differ in the heuristics used. A drawback of both methods is that they do not identify small clusters of similar anomalies. The RI-DISCORD method attempts to resolve this by extending the definition of discords to be the top  $m$  examples with the largest distance to its  $k$ th nearest neighbor. However, this requires one to know in advance the value of  $k$  that is inclusive of small anomalous clusters.

Because RI-DISCORD is the only anomaly detection method that is designed to handle unphased data without the use of a reference set, we compare PCAD's performance to RI-DISCORD in Sect. 8. Note that RI-DISCORD is designed to find global anomalies only. It does not discover local anomalies.

### 3 The challenge of unphased data

One may reasonably ask whether any of the methods cited in Sect. 2 can be adapted or applied to handle unsynchronized time series data. The answer is no for methods that perform feature transformations that do not respect the time domain (Aggarwal and Yu 2001; Lazarevic and Kumar 2005). These methods would not work for time series data in general. For methods that rely on spatial indexes (Ramaswamy et al. 2000), one would need to synchronize or *universally phase* the data before applying the anomaly detection method. We discuss universal phasing at the end of this section.

The other way to adapt a general outlier detection method is to use cross correlation, a distance metric for which there exists an efficient method for computing the optimal phase shift that maximizes the similarity between two time series. For time series  $x$  and  $y$ , cross correlation is computed

$$r_{xy}^2(\tau) = \sum_{t=0}^{d-1} x(t)y(t-\tau), \quad (1)$$

where  $t$  is discrete time,  $d$  is the number of time points and  $\tau$  is the phase shift. A phase shift implies a rotation of the times series. If  $t - \tau < 0$ , we wrap the time series around and let  $y(t - \tau)$  equal  $y(t - \tau + d)$ . Finding the max of  $r_{xy}^2(\tau)$  requires finding the value of  $\tau$  that maximizes cross correlation. The running time of a brute force search for the optimal  $\tau$  is  $O(d^2)$ . Fortunately, we can use the convolution theorem to find the same value in  $O(d \log d)$ . According to the convolution theorem, cross correlation can be written as

$$r_{xy}^2(\tau) = \mathcal{F}^{-1}[\mathcal{X}(v)\overline{\mathcal{Y}(v)}](\tau)$$

where  $\mathcal{X}(v)$  is the Fourier transform of  $x(t)$  and  $\overline{\mathcal{Y}(v)}$  is the complex conjugate of the Fourier transform of  $y(t)$ . One finds the maximum correlation by finding the maximum of the inverse Fourier transform of the product of the Fourier transforms of the two time series. For fast Fourier transforms (FFT), each Fourier transform requires  $2d \log d$  operations for any value  $d$ . Thus, the calculation of cross correlation of a pair of time series is  $O(d \log d)$ .

Simply substituting cross correlation maximized over all possible phase shifts, or *maximized cross correlation*, as the distance metric into a general outlier detection method may not yield desirable results for unsynchronized time series data. First, the use of maximized cross correlation increases the computational expense of distance calculations from  $O(d)$  to  $O(d \log d)$ , a non-trivial expense if repeated  $k$ -nearest neighbor calculations are performed on high-dimensional data (Bay and Schwabacher 2003; Keogh et al. 2005). This cost might be absorbed by methods running on data sets where  $n \gg d$ . However, a method that aggregates the results of distance calculations (e.g., averaging) (Jin et al. 2001) on a subset of the data must contend with the set of unique phase shifts for every pair of time series in that group, and possibly rephase individual time series before performing those calculations. One may need to redesign the method to intelligently handle these issues.

Universal phasing is the global synchronization of the data set, after which, an out-of-the-box anomaly detection method can be applied. The simplest universal phasing algorithm aligns a set of times series by setting the maximum (or minimum) of each time series to time  $t$ . Protopapas et al. developed a more robust version of this method that accounts for noise (Protopapas et al. 2006). Rather than phase each time series to its maximum, the method sorts the values of the time series and isolates the highest and lowest ten percent. Those values are then separated into two clusters. Time  $t$  is set to the mean value of the cluster containing the higher (or lower) values. For full details on how universal phasing is performed, please refer to Protopapas et al. (2006).

The drawback of universal phasing is that it does not work for all data sets. Specifically, it will not work if the data set contains time series with multiple maxima (and minima) of the same height (give or take noise). Under those circumstances, the phasing algorithm will arbitrarily choose one peak and set that to time  $t$ . Similarity calculations will be incorrect if performed on time series that do not universally phase well.

For some data sets, the general shape of the time series is known and universal phasing is appropriate. However, for large sets of time series containing an unknown classes of objects, the use of universal phasing poses a risk. The imminent release of the Pan-STARRS project

underscores this urgency. Billions of light-curves of unknown class are forthcoming. There is no guarantee that the shape of all objects from this survey will meet the requirements for universal phasing. Given the pending volume and diversity of this project, it is prudent to use a method that makes no assumptions on the shape of the time series, and whose computational expense already accounts for the cost of phasing.

## 4 PCAD

PCAD, an acronym for Periodic Curve Anomaly Detection, is our anomaly detection technique for sets of unsynchronized periodic time series. PCAD does not use a reference data set of normal examples. Instead, it uses unsupervised learning on a sampling of the data to generate a set of centroids that are representative of the data. The local and global anomaly scores for a time series is based on its similarity to this set of centroids.

We implement a modified k-means algorithm as our unsupervised technique. Our modification solves the phasing issue by rephasing each time series to its closest centroid before recalculating the centroid at every iteration. Our algorithm, Pk-means, produces a set of  $k$  centroids that are used to calculate the local and global anomaly scores. The end user may sort the time series data according to his desired anomaly score and obtain a ranked set.

We first review the k-means algorithm before describing the Pk-means algorithm in-depth. We then discuss the computational expense of Pk-means and how sampling the data improves the overall efficiency of PCAD. We then discuss the final step of PCAD, outlier score calculation, and provide scoring functions for both local and global outliers.

### 4.1 Review of k-means

Given a set of  $n$  data points, k-means begins by initializing the cluster centers to a set of  $k$  points randomly selected from the data. It then calculates the similarity between each data point and each centroid, (re)assigns each point to its closest centroid, and then calculates a new centroid for each cluster by averaging the points in the cluster. The algorithm repeats from the similarity calculation step until a convergence criterion is met (e.g., clusters no longer change).

The time complexity of k-means in  $O(knrd)$  where  $n$  is the number of data points (or time series, in our case),  $k$  is the number of centroids,  $r$  is the number of iterations until convergence and  $d$  is the number of features, which in our case, is the number of points in the time series. In order to run k-means, the user must either supply the value of parameter  $k$ , or use a model selection criterion such as the Akaike Information Criterion or the Bayesian Information Criterion (Pelleg and Moore 2000) to automatically determine an appropriate value of  $k$ .

### 4.2 Pk-means

In Fig. 3 we show the pseudo-code for Pk-means. The initialization and cluster assembly subtasks remain unchanged from k-means. Convergence is achieved when cluster composition does not change upon successive iterations. We discuss convergence in detail in Sect. 5.

Figure 4 shows the distance calculation subroutine used by Pk-means. For each time series  $x[i]$ , we calculate maximized cross correlation between it and each of the  $k$  centroids. We determine which centroid is most similar to  $x[i]$  and store the phase adjustment required to produce the maximum correlation. The centroid numbers are stored in the array

```

1: Pk-means(Time Series Set: x[], Number of centroids: k)
2: Initialize centroids[]
3: while !AchievedConvergence do
4:   best_centroids[]  $\leftarrow$  CalcDistance(x[], centroids[])
5:   clusters[][]  $\leftarrow$  AssembleClusters(x[], best_centroids[])
6:   centroids[]  $\leftarrow$  RecalcCentroids(clusters[][])
7: end while
8: return centroids[]

```

**Fig. 3** Algorithm for Pk-means. Data structures followed by a [] denote list or array structures

```

1: CalcDistance(Time Series set: x[], Centroids: centroids[])
2: for  $i = 1$  to  $n$  do
3:   max_corr[ $i$ ]  $\leftarrow$  0
4:   for  $j = 1$  to  $k$  do
5:     ( $corr, phase$ )  $\leftarrow$  CalcCorrelationFFT(x[ $i$ ], centroids[ $j$ ])
6:     if max_corr[ $i$ ] < corr then
7:       max_corr[ $i$ ]  $\leftarrow$  corr
8:       best_center  $\leftarrow$   $j$ 
9:       best_phase  $\leftarrow$  phase
10:    end if
11:  end for
12:  best_centroids[ $i$ ]  $\leftarrow$  best_center
13:  x[ $i$ ]  $\leftarrow$  UpdatePhase(lc[ $i$ ], best_phase)
14: end for
15: return best_centroids[]

```

**Fig. 4** Algorithm for the distance calculation subroutine of Pk-means. Data structures followed by a [] denote list or array structures

*best\_centroids*[] and used for cluster assignment in the next step of Pk-means. However, before exiting the distance calculation subroutine,  $x[i]$  is rephased according to the phase adjustment needed to maximize its correlation to the centroid.

This last step is critical; upon each iteration, Pk-means adjusts the phase of each time series. In k-means, the data points never change; centroid calculation is only affected by cluster membership. In Pk-means, each centroid is determined by its cluster membership and the phase adjustments of the time series in its cluster. Thus, Pk-means is not merely k-means using cross correlation as a distance metric. Figure 5 shows examples of centroid light-curves output by Pk-means.

As with k-means, the parameter  $k$  must be specified in advance. We search across multiple values of  $k$  and select the optimal  $k$  using the Bayesian Information Criterion (BIC). BIC is calculated according to the method outlined in Pelleg and Moore (2000). The set of centroids produced from this run of Pk-means is used to calculate the anomaly scores for all light-curves in the data set.

#### 4.3 Sampling and computation time

The time complexity of Pk-means is  $O(knr d \log d)$  where  $n$  is the number of time series,  $k$  is the number of centroids,  $r$  is the number of iterations until convergence,  $d$  is the number

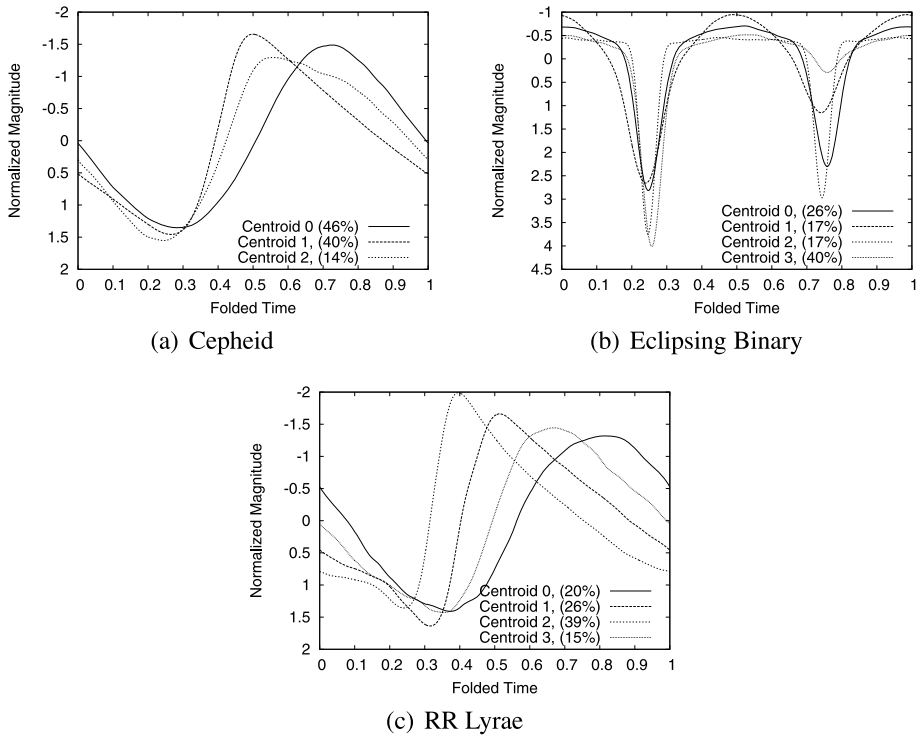


**Fig. 5** Centroid output of Pk-means. The number in parentheses is the percentage of the data assigned to that cluster. The parameter  $k$  equals 3, 4 and 4 in these figures respectively. In our experiments,  $k$  is chosen using the Bayesian Information Criterion (BIC)

of points in a single time series, and  $d \log d$  is the cost of computing cross correlation using a FFT. Because  $d$  and  $k$  are independent of  $n$ , we can reduce the time complexity to  $O(nr)$ .

Time series methods must be  $O(n)$  in order to scale to large data sets. At  $O(nr)$ , Pk-means does not meet this requirement. However, recall that the goal of Pk-means is to produce a set of centroids that is representative of the data. Given a large data set, it may be possible to generate this representative set from a random sampling of size  $s$  where  $s \ll n$ . This reduces the time complexity of Pk-means with respect to the overall data set size. Additionally, we can perform Pk-means (as well as the associated search for the optimal  $k$ ) offline. In Sect. 8.3, we present empirical results that support the intuition that sampling the data to find the centroids has little impact on the rankings of the anomalies.

The online portion of PCAD is simply the anomaly score calculation. A local and global anomaly score can be simultaneously calculated for each time series in the data set. The anomaly score calculation uses the FFT method of calculating maximized cross correlation between each time series and the centroids output by Pk-means. Thus, the computation time of the anomaly score calculation is  $O(knd \log d)$  which reduces to  $O(n)$ . Thus, the online portion of PCAD is linear in the size of the data set.

#### 4.4 Local and global anomaly scores

We calculate the anomaly score for a time series in relation to the  $k$  centroids returned by Pk-means. If one seeks global anomalies, then the anomaly score for time series  $x[i]$  or  $x_i$  is calculated:

$$score(x_i) = \sum_{j=1}^k \frac{|c_j|}{n} r_{x_i, c_j}^2 \tag{2}$$

where  $c_j$  is a centroid,  $|c_j|$  is the number of time series closest to  $c_j$ , and  $n$  is the size of the data set. The lower the score, the more anomalous the time series is with respect to the entire data set. We use a weighted average to offset the influence of relatively small clusters.

To find local anomalies, the anomaly score is the distance of a time series to its closest centroid. This is computed as:

$$score(x) = \min_j r_{x, c_j}^2 \tag{3}$$

After an anomaly score is calculated for each time series, the time series are sorted in order of ascending scores. For global anomalies, the top  $m$  time series (where  $m$  is specified by the user) are returned as the list of anomalies. For local anomalies, we isolate the top  $m$  anomalies per cluster.

### 5 Pk-means convergence

In this section we prove that Pk-means, and its use of maximized cross correlation, does not break the convergence properties of k-means. We first review the proof of convergence for k-means and then prove the convergence of Pk-means.

#### 5.1 Review of proof of convergence of K-means

The following proof of k-means' convergence has been adapted from Bottou and Bengio (1995). Please note that we have slightly changed the notation.

If we review the steps of k-means, we see that each iteration begins with a set of centroids  $W$ , which are either the  $k$  centroids k-means is initialized with, or the centroids calculated during the previous iteration. Within each iteration of k-means, a new set of clusters  $C$  is assembled based on each data point's proximity to the centroids  $W$ . From  $C$ , a new set of centroids  $W'$  is calculated, from which new cluster assignments,  $C'$ , are made. Thus, k-means progresses from

$$W \rightarrow C \rightarrow W' \rightarrow C'$$

We define the quantization error  $E(W, C)$  in relation to  $W$  and  $C$  as follows:

$$\begin{aligned} E(W, C) &= \sum_i \frac{1}{2} \min_{w \in W} (x_i - w)^2 \\ &= \sum_i \frac{1}{2} (x_i - w_{c(i)})^2 \end{aligned} \tag{4}$$

where  $x_i$  is a data instance,  $w$  is the centroid in  $W$ , and  $c(i)$  is the cluster to which  $x_i$  is assigned.

K-means converges if, at each iteration, the quantization error is non-increasing. To show that the quantization error is non-increasing, we must prove  $E(W', C') \leq E(W, C)$ , or

$$\sum_i \frac{1}{2}(x_i - w'_{c'(i)})^2 \leq \sum_i \frac{1}{2}(x_i - w_{c(i)})^2$$

To show that the error decreases between  $E(W, C)$  and  $E(W', C')$ , we demonstrate that  $E(W', C') \leq E(W', C) \leq E(W, C)$ . This decreasing progression corresponds to the steps of the k-means algorithm. The term  $E(W', C)$  corresponds to the decrease in error that results after calculating the new centroids, while maintaining the old cluster assignments, where

$$E(W', C) = \sum_i \frac{1}{2}(x_i - w'_{c(i)})^2$$

The term  $E(W', C')$  results after the cluster assignments are updated so that each point is assigned to the cluster of its closest centroid under  $W'$ .

In the k-means algorithm, the new centroids  $W'$  are calculated by averaging the points in each of the clusters in  $C$ . This definition of  $W'$  is the one that minimizes  $E(W', C)$ . We find the value for  $w' \in W'$  by computing  $\delta E / \delta w'$ , setting the resulting expression equal to 0, and solving for  $w'$ :

$$w' = \frac{1}{|c|} \sum_{i \in c} x_i$$

where  $c \in C$ . Since by definition  $W'$  are centroids that minimize the cluster assignments based on the previous  $C$ ,  $E(W', C) \leq E(W, C)$  holds.

Having calculated the new centroids  $W'$ , new cluster assignments  $C'$  are made with respect to  $W'$  to minimize the distance between each  $x_i$  and its closest centroid  $w'_{c'(i)}$ , yielding

$$\sum_i \frac{1}{2}(x_i - w'_{c'(i)})^2 \leq \sum_i \frac{1}{2}(x_i - w'_{c(i)})^2$$

which means  $E(W', C') \leq E(W', C)$ . Thus, we've shown the quantization error decreases at every iteration by  $E(W', C') \leq E(W', C) \leq E(W, C)$ . Finally, because there are a finite number of data points and cluster assignments, k-means must converge.

### 5.2 Convergence of Pk-means using squared distance

We demonstrate that Pk-means converges using the squared distance metric. In Sect. 5.3, we establish the relationship between cross correlation, the distance metric of Pk-means, and squared distance.

Recall from Sect. 4.2 that Pk-means differs from k-means in two ways. First, Pk-means searches across all phase shifts  $\{\tau\}_0^{d-1}$  when calculating distance between a time series  $\mathbf{x}_i$  and centroid  $\mathbf{w}$ . Second, once Pk-means finds the centroid  $\mathbf{w}_c(i)$  and phase shift  $\tau_i$  that minimizes distance, Pk-means horizontally adjusts  $\mathbf{x}_i$  by  $\tau_i$  and produces  $\mathbf{x}_i^{\tau_i}$ . We refer to the collective set of phase adjustments with respect to centroids  $W$  as  $T$ . If phase adjustments are done with respect to  $W'$ , we refer to these as  $T'$  and  $\tau'_i$ .

In Fig. 3, distance calculation and cluster assembly are listed as separate steps since algorithmically they populate different data structures. However, distance calculation implies

cluster composition since finding the closest centroid to  $\mathbf{x}_i$  effectively assigns that time series to a cluster. Thus, phase shifts  $T$  and cluster assignments  $C$  are determined simultaneously. We represent this relationship as tuple  $(T, C)$ . Thus, Pk-means progresses from:

$$W \rightarrow (T, C) \rightarrow W' \rightarrow (T', C')$$

In order for Pk-means to converge, its quantization error must also be non-increasing at each iteration. To incorporate the effects of phase changes on the quantization error, we define the quantization error for Pk-means as

$$E(W, (T, C)) = \sum_{i=1}^n \frac{1}{2} (\mathbf{x}_i^{T_i} - \mathbf{w}_{c(i)})^2$$

Thus, our goal is to prove that  $E(W', (T', C')) \leq E(W, (T, C))$ . We do this by proving that  $E(W', (T', C')) \leq E(W', (T, C)) \leq E(W, (T, C))$ . Before we prove both expressions, we must derive the value of  $\mathbf{w}' \in W'$  under Pk-means. This is the value that minimizes  $E(W', (T, C))$ . Taking the first derivative of this expression with respect to  $\mathbf{w}'$ , setting it equal to zero, and solving for  $\mathbf{w}'$ , we get

$$\mathbf{w}' = \frac{1}{|c|} \sum_{i \in c} \mathbf{x}_i^{T_i} \tag{5}$$

The centroids  $W'$  that minimize  $E(W', (T, C))$  are obtained by averaging the time series belonging to clusters  $C$  but with the added constraint that the data are phased according to  $T$ . This is exactly how Pk-means calculates the new centroids. Since by definition,  $W'$  are the centroids that minimize the distance of the data with respect to  $(T, C)$ ,  $E(W', (T, C)) \leq E(W, (T, C))$ .

After  $W'$  is calculated, we find the  $T'$  and  $C'$  that minimize the distance of each  $x_i$  to its closest centroid  $\mathbf{w}'_{c'(i)}$ . From this,  $E(W', (T', C')) \leq E(W', (T, C))$  follows. Thus, we have shown that the quantization error is non-increasing under the phase changes of Pk-means.

### 5.3 Cross correlation versus squared distance

Having shown that Pk-means converges using squared distance, we show that Pk-means converges using cross correlation by establishing the relationship between cross correlation and squared distance. Recall the definition of cross correlation in (1). The following equation demonstrates that, if the vectors are normalized, squared distance and cross correlation are inversely related.

$$\begin{aligned} \frac{1}{2}(\mathbf{x} - \mathbf{y})^2 &= \frac{1}{2}(\mathbf{x} \cdot \mathbf{x} - 2\mathbf{x} \cdot \mathbf{y} + \mathbf{y} \cdot \mathbf{y}) \\ &= \frac{1}{2}(1 - 2\mathbf{x} \cdot \mathbf{y} + 1) \\ &= 1 - \mathbf{x} \cdot \mathbf{y} \\ &= 1 - r_{xy}^2 \end{aligned}$$



We show that using cross correlation does not impact the calculation of the centroids  $W'$  by substituting the (negated) definition of cross correlation into expression  $E(W', (T, C))$ :

$$\begin{aligned} & \sum_i \sum_{t=0}^{d-1} -w'_{c(i)}(t) \cdot x_i(t - \tau_i) \\ &= \sum_i \left( \frac{1}{2} (\mathbf{x}_i^{\tau_i} - \mathbf{w}'_{c(i)})^2 - 1 \right) \\ &= \sum_i \left( \frac{1}{2} (\mathbf{x}_i^{\tau_i} - \mathbf{w}'_{c(i)})^2 \right) - n = E(W', (T, C)) - n \end{aligned}$$

Cross correlation changes the expression of  $E(W', (T, C))$  only by the subtraction of  $n$ . Thus, centroid calculation remains unchanged under cross correlation, and the convergence of Pk-means using cross-correlation follows from the proof of Pk-means convergence using squared distance.

## 6 Data

Before moving to our experimental results, we describe the four time series data sets we experimented with. Three are non-astronomy data sets. The fourth data set is our motivating application: light-curve data from the astronomy domain. We briefly describe the three non-astronomy data sets, and discuss in-depth the source, generation and pre-processing of our light-curve data.

### 6.1 Non-astronomy time series data

The first non-astronomy time series data set, referred to as *nose*, was generated by the Walt Laboratory at Tufts University. Each example was generated in the laboratory by passing a vapor over a succession of sensors. The full data set contains eight classes (vapors) with fifteen examples each. The length of each time series is eighty time points.

The second data set, referred to as *mallat*, is a synthetic data set generated by Mallat (1998) for the study of wavelets in signal processing, and is available at the UCR time series data archive (Keogh and Folias 2002). The full data set contains eight classes numbering 300 examples each. Each example is 1024 time points.

The third data set, referred to as *landcover* was donated by Dr. Mark Friedl of Boston University. This data set consists of time series of satellite observations of the earth's surface. There are a total of 18 classes, with each example containing 135 time points. Note that the class distribution is not uniform.

In the state provided to us, these data sets are perfectly synchronized. The reason they were selected for experimentation is that they serve as examples of the shapes of time series for which universal phasing does not work (see Sect. 3). We simulate the phasing problem by randomly rephasing (rotating) each time series. We then universally phase each randomly-rephased curve to create the universally-phased version of those data sets. Thus, our experiments are run on both randomly-phased and universally-phased data. The only pre-processing performed on these data sets was  $z$ -score normalization, which was done prior to the random- and universal-phasing.

## 6.2 Light-curve data

The source of the light-curve data is the Optical Gravitational Lensing Experiment Survey (Udalski et al. 1997). We refer to this data as *ogle*. The telescopes used for this survey capture CCD images of the night sky over time. Each digital image is carved into “tiles” and the stars in each tile are identified by number. An astronomer converts the series of image data for each star into a light-curve—a real-valued series measuring the magnitude of light in each image and its associated observational error. In order to keep our algorithm generic to univariate time series data, PCAD uses only the light magnitude measurement. The result of not incorporating observational errors into PCAD is that an otherwise typical light-curve with noisy measurements may appear anomalous. We take the observational errors into account when the astronomers analyze the ranked output from PCAD. Because this increases the time an astronomer must spend analyzing PCAD output, in future work we will automate the handling of light-curves with high observational errors.

Because we work with periodic stars, we are able to transform the photometric time series produced by the observing team of astronomers into a single light-curve in which each period is mapped onto the same time axis as follows:

$$t' \equiv \left\{ \frac{t - t_0}{T} \right\} \quad (6)$$

where  $T$  is the period,  $t_0$  is an arbitrary starting point and the symbol  $\{ \}$  represents the non-integer part of the fraction. This process produces a *folded light-curve* on an  $x$ -axis of *folded time* that ranges from 0 to 1. In the *ogle* data sets, the lengths of the folded light-curves range between 200 to 500 time points. The purpose of folding is to produce a stronger, more consistent signal. Figure 6 shows an example of an Eclipsing Binary light-curve before and after folding.

The data are pre-processed according to a technique developed by Protopapas et al. (2006). We refer the reader to Protopapas et al. (2006) for an in-depth discussion of each technique and its parameters. In brief, we conservatively pre-process the data using spike removal, smoothing, interpolation and normalization. Spike removal and smoothing is used to eliminate time points that are individually noisy, while preserving interesting features. We use interpolation because PCAD uses a FFT, which requires the time points of each light-curve to be uniformly spaced. Finally, we use  $z$ -score normalization to ensure similarity cal-

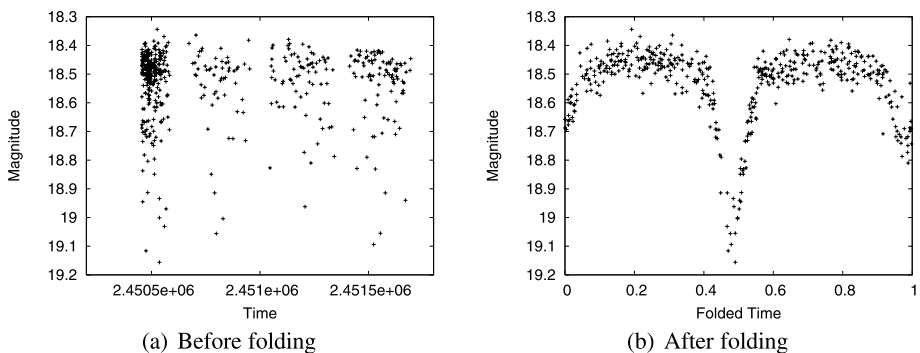


**Fig. 6** An Eclipsing Binary light-curve before and after folding. Note that after folding the  $x$ -axis ranges from 0 to 1 because only the non-integer part of the original time points are kept

culations are meaningful. The pre-processing done on the light-curves is domain-specific, and not part of the PCAD technique. Whether time series from other domains must undergo pre-processing is the decision of a domain expert for that data set.

The data are folded light-curves, which we simply refer to as light-curves. Our data sets consist of 1329 Cepheid (CEPH), 2580 Eclipsing Binary (EB) and 5327 RR Lyrae (RRL) light-curves, with each data set containing an unknown number of anomalies.

There are some important characteristics of these data sets that have bearing on our experimental results. The first is that the variance on the EB data set is eight times the variance of either CEPH or RRL. The second is that despite CEPH and RRL being distinct star classes, the shapes of their light-curves are very similar (refer to Fig. 1 for examples of both). Indeed, domain experts resort to other data sources to classify CEPH and RRL light-curves correctly. Due to the similarity in the shape of the light-curves, time series anomaly detection methods, including ours, have difficulty distinguishing between CEPH and RRL.

## 7 Experiments

Our main experimental goal is to justify the expense of PCAD by comparing it to a variety of naive solutions. The second goal is to evaluate PCAD's performance as an approximation of a published anomaly detection for light-curve data, and compare PCAD to other approximations of this benchmark.

### 7.1 Alternatives to PCAD

Due to the lack of published alternatives to PCAD, we propose several anomaly detection methods for handling large sets of unsynchronized data that are both simpler and cheaper than PCAD. The first method samples  $k$  examples uniformly from the data set to generate a reference set of "centroids", instead of running an expensive algorithm like k-means or Pk-means. One can then calculate the outlier score using maximized cross correlation against this randomly selected set. We call this method RAND-CC. Please note that for RAND-CC, sample size and centroid size are the same.

Another alternative is to set  $k = 1$  in Pk-means and generate a single centroid from which the outlier scores are calculated. This solution, P1-MEAN, precludes finding local outliers, but may be an acceptable solution for finding global outliers. P1-MEAN has a cost of  $O(n)$  for both centroid and outlier score calculation.

Our final naive alternatives to PCAD are KMEANS-ED and KMEANS-CC. K-means is a viable alternative to PCAD when run on universally-phased data. K-means is clearly cheaper than Pk-means because it lacks the  $\log d$  factor required by the FFT. KMEANS-ED uses k-means to generate centroids and uses Euclidean distance to calculate the outlier scores. KMEANS-CC also uses k-means to generate centroids, and uses maximized cross correlation to calculate the outlier scores.

As a final point of comparison, we compare PCAD to the RI-DISCORD method described in Sect. 2. We implemented the brute-force version of RI-DISCORD, as we are interested in comparing performance rather than computational speed. We also implement RI-DISCORD using maximized cross correlation as the distance metric, which is equivalent to the  $O(n^2)$  measure of finding the minimum distance over all possible rotations. We define discords to be the examples with the farthest nearest neighbor.

## 7.2 Benchmark and approximations

On the ogle data set we compare PCAD's performance to a robust solution called PN-MEANS (Protopapas et al. 2006). This is a method published in an astrophysics journal for light-curve data specifically. It is also an exhaustive version of PCAD where  $k$  is set to  $n$  (the number of light-curves in the data set) and no sampling is performed. The anomaly score calculated for each light-curve is the weighted average of its similarity to the other  $n - 1$  light-curves. The weights are Gaussian, with the sample mean and standard deviation of the  $n - 1$  correlations plugged in as parameters. Note that PCAD differs from PN-MEANS in the weights used for outlier score calculation. While PN-MEANS uses Gaussian weights, PCAD uses proportional cluster sizes as weights. We decided against using Gaussian weights for PCAD because PCAD calculates the outlier scores from a small number of typical-looking centroids. Gaussian weighting is useful when the outlier score is calculated from a larger, more diverse group of correlation scores.

By doing an exhaustive pair-wise comparison of the light-curves, PN-MEANS is the most precise anomaly score that PCAD can calculate. Hence, we consider PN-MEANS to be PCAD's benchmark. However, because PN-MEANS sets  $k = n$ , it is  $O(n^2)$ . Thus, PCAD is an improvement over PN-MEANS in terms of computational expense, rather than quality of results.

We compare PCAD's ability to approximate PN-MEANS to two others approximations of PN-MEANS. The first method, called Protopapas\_n, is an  $O(n)$  approximation of PN-MEANS that calculates the outlier score of each light-curve in relation to a single centroid, calculated by averaging the examples in the data set (Protopapas et al. 2006). This is similar to P1-MEAN except that correlation rather than maximized cross correlation is used as a distance metric. The second method is RAND-CC, which can also be thought of as an approximation of PN-MEANS. While PN-MEANS builds a  $n \times n$  similarity matrix and calculates the outlier score by doing a weighted Gaussian averaging the columns, RAND-CC builds a  $r \times n$  similarity matrix where  $r$  is the cardinality of a randomly-selected subset of the data. The outlier score calculation for RAND-CC is identical to PCAD in that it is a weighted average of a time series' correlation to each of the randomly-selected centroids, where the weights are the proportion of the  $n$  light-curves that are closest to each centroid. We also created a second version of RAND-CC, called RAND-CC-GAUSS, which differs from RAND-CC in that it uses Gaussian weighting to calculate the outlier score instead of cluster proportions. We compare PCAD to Protopapas\_n, RAND-CC, and RAND-CC-GAUSS to show that PCAD is the better approximation of PN-MEANS.

## 7.3 Summary of experimental goals

Having described the methods to which we compare PCAD, we summarize our experimental goals as follows:

- Evaluate PCAD's effectiveness in comparison to the alternatives described above (KMEANS-ED, KMEANS-CC, P1-MEAN, RAND-CC and RI-DISCORD) on randomly-phased data that contains a known number of anomalies.
- Evaluate the same methods on the universally-phased versions of the data.
- Determine whether PCAD is a better approximation of PN-MEANS than either Protopapas\_n, RAND-CC, and RAND-CC-GAUSS on light-curve data containing an unknown number of anomalies.
- Understand the effect of parameter  $k$  and sampling on PCAD's rankings.
- Provide an astrophysicist's analysis of the anomalies found by PCAD.

## 8 Results

### 8.1 Data with known anomalies

We created data sets with known numbers of anomalies from each of the four data sets we introduced in Sect. 6. To create data sets with global anomalies, we mixed examples from three classes together. The first two classes are the “normal” classes. They are similar classes, and comprise 95% of the synthetically-mixed data set. The remaining 5% of the data are instances from an “outlier” class, which is a class that is dissimilar to the other two. We selected our class mixes either through domain expert advice or from visual inspection of the data. For the nose data set, ‘hep’ and ‘tol’ were selected as the normal classes, and ‘decoh’ as the outlier class. For the landcover data set, we selected ‘Woody Savanna’, and ‘Cropland’ as the normal classes, and ‘Snow-Ice’ as the outlier class. For the mallat data set, classes 3 and 6 are the normal classes, and class 7 is the outlier class. For the ogle data set, CEPH and RRL are the normal classes, and EB is the outlier class. The sizes of the synthetically-mixed global anomaly data sets are 32, 210, 1050 and 1050 for nose, mallat, landcover and ogle respectively.

To create data sets with local outliers, we mixed examples from four classes. Two classes are “normal” classes and comprise 95% of the data. However, these two classes are dissimilar and should not cluster together. The remaining two “outlier” classes comprise 5% of the data. Each outlier class is similar to one of the normal classes, and dissimilar to the other. Thus, each outlier class should be a local outlier with respect to one of the normal classes only. For the nose data set, ‘tol’ is a local outlier with respect to ‘hep’, and ‘decoh’ is a local outlier with respect to ‘diesel’. For the mallat data set, classes 3 and 6 form one normal/outlier pair, and classes 7 and 2 form another. For the landcover data set, Croplands/Woody Savanna form one pairing, and Open Shrubland/Snow-Ice another. Because the ogle data set contains only three classes, it could not be used to create a synthetically-mixed data set for local outliers. The sizes of the synthetically-mixed local anomaly data sets are 32, 210, and 1050 for nose, mallat, and landcover respectively.

Because we know that the true number of anomalies in each data set is  $m$ , we look at the top  $m$  entries in each method’s output and measure precision. Because there are  $m$  true anomalies and  $m$  reported anomalies in these experiments, precision and recall are equal. Thus, we report only one number. We performed ten iterations of each experiment. In each iteration, we created a data set in the proportions described above via random sampling. For the global outlier experiments, we experimented with values of  $k$  between 1 and 7, and selected the optimal  $k$  values for k-means and Pk-means using BIC. For RAND-CC, we set the reference set or “centroid” size to the value returned by BIC for Pk-means. For example, if, for a given experimental iteration, PCAD calculated the outlier score against four centroids, then RAND-CC will calculate its outlier score against four randomly-sampled light-curves.

For the local anomaly experiments, we set  $k = 2$  to force the evaluation of local outliers with respect to two clusters. P1-MEAN is omitted from the local outlier experiments because it calculates only one centroid. RI-DISCORD is also omitted because it finds only global outliers.

We also demonstrate the effect of sample size on the results of KMEANS-ED, KMEANS-CC, P1-MEAN, and PCAD by running both k-means and Pk-means with sample sizes that are 5, 10, 20, 30, 40, 50 and 100% of the synthetically-mixed data sets. Because the synthetically-mixed nose data set is too small to be sampled (32 examples), we ran Pk-means on all thirty-two examples. We ensure that the same centers—in one case randomly-phased, in the other universally-phased—initialize k-means and Pk-means for each experimental iteration. We performed the random-phasing by choosing an arbitrary time point in each time

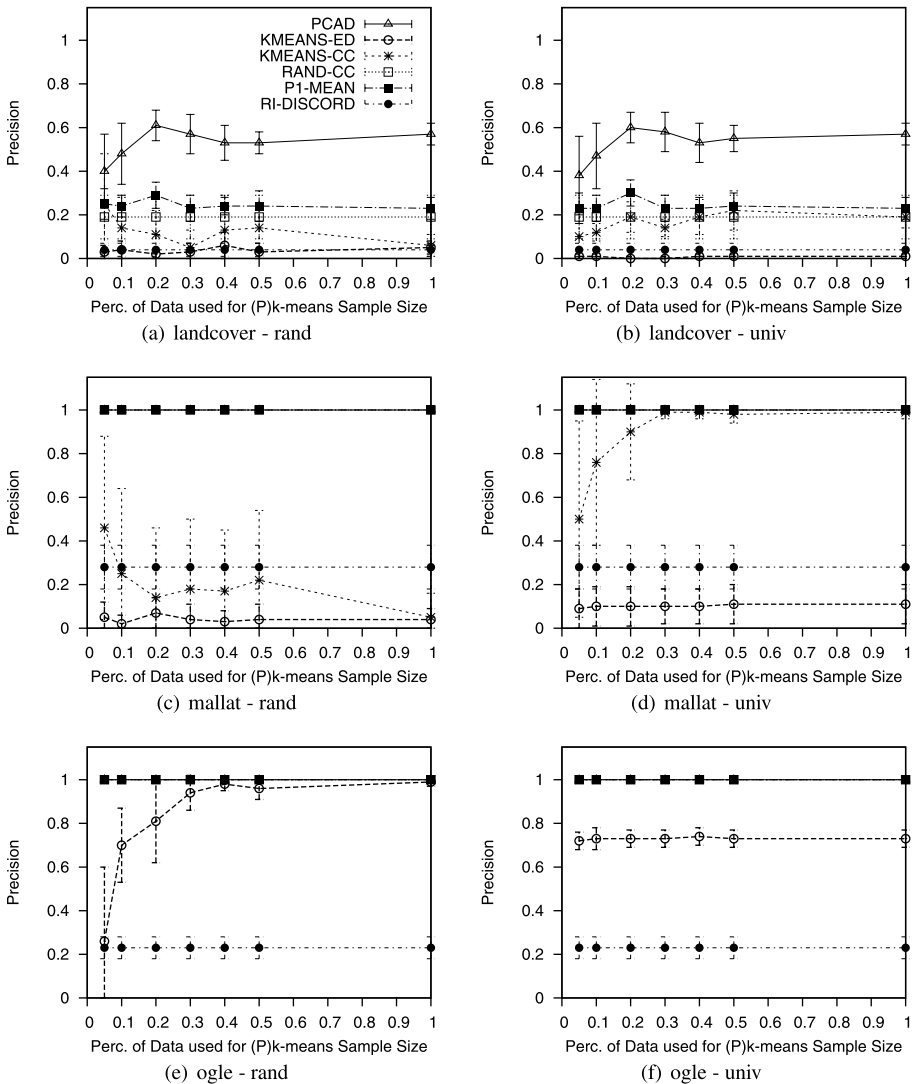


**Fig. 7** Precision vs. sample size for each data set synthetically-mixed to have *global* outliers. The *x*-axis measure the percentage of the data set used in the sampling given to either *k*-means or PK-means. The *left-hand column* shows results for randomly-phased data. The *right-hand column* shows results for universally-phased data. Note that because RAND-CC and RI-DISCORD do not have a (P)*k*-means subroutine, their results do not vary over the *x*-axis

series, and rotating the time series such that this chosen time point becomes the starting point (time zero). The ogle data set is naturally unsynchronized, and has no need for random phasing. Thus, experiments labeled ‘rand’ for ogle refer to the time series in their original form. Universal phasing is performed according the method specified in Protopoulos et al. (2006).

Figures 7, 8, and 9 plot the mean precision versus sample size on the randomly- and universally-phased data sets of landcover, mallat and ogle. All results for nose are reported

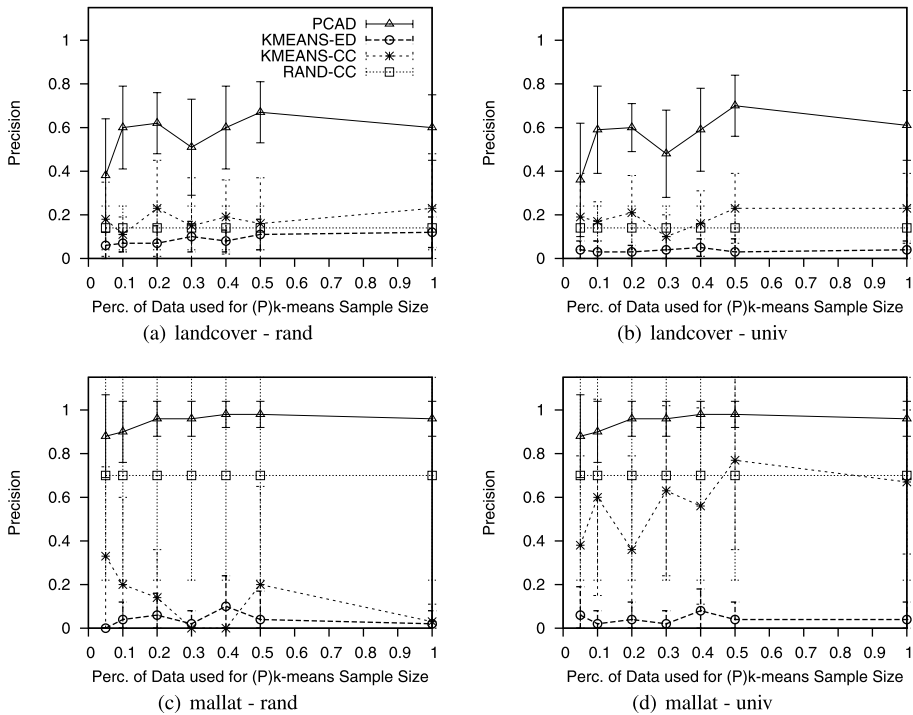


**Fig. 8** Precision vs. sample size for each data set synthetically-mixed to have *local* outliers. Results are for local outliers with respect to *centroid 1*. The *x*-axis measure the percentage of the data set used in the sampling given to either k-means or Pk-means. The *left-hand column* shows results for randomly-phased data. The *right-hand column* shows results for universally-phased data. Note that because RAND-CC does not have a (P)k-means subroutine, its results do not vary over the *x*-axis

in Table 1. Because RAND-CC and RI-DISCORD do not use k-means or Pk-means to generate centroids, we show their results as a straight line in each plot. Also, because RAND-CC and RI-DISCORD use maximized cross correlation to calculate the outlier score, the results for RAND-CC and RI-DISCORD are identical for randomly- and universally-phased data. PCAD and P1-MEAN also use maximized cross correlation, but are not guaranteed to have identical results between randomly- and universally-phased data because the intermediate step of centroid calculation is done with differently-phased time series. Nevertheless, the results are very similar. KMEANS-CC's and KMEANS-ED's results change more dramatically between randomly- and universally-phased data.

Our first observation is that PCAD performs best overall. In global anomaly experiments, it performs perfectly on the nose, mallat and ogle for both randomly- and universally-phased data. On all other experiments, local and global, it is the best performing method with one exception (the 'lcl.1' experiment on randomly-phased nose data).

The methods that perform most poorly are KMEANS-ED and RI-DISCORD. The poor performance of KMEANS-ED is expected considering there is no attempt to phase the data in either the centroid or outlier score calculation. Thus, its results are poor for both randomly and universally-phased data. Surprisingly, KMEANS-ED shows good results on the synthetically-mixed ogle data set for global outliers. There are two reasons for this. The first is that it is very easy to distinguish EB, the minority light-curve in this data set, from both

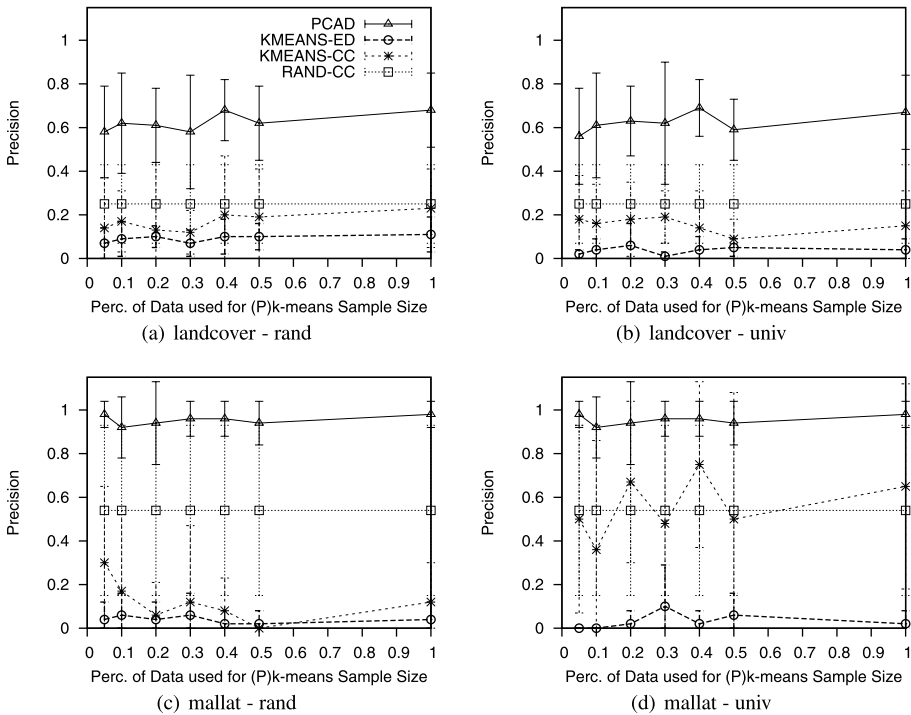


**Fig. 9** Precision vs. sample size for each data set synthetically-mixed to have *local* outliers. Results are for local outliers with respect to *centroid 2*. The *x*-axis measure the percentage of the data set used in the sampling given to either *k*-means or *Pk*-means. The *left-hand column* shows results for randomly-phased data. The *right-hand column* shows results for universally-phased data. Note that because RAND-CC does not have a *(P)k*-means subroutine, its results do not vary over the *x*-axis

**Table 1** All precision results for the nose data set. ‘gbl’, ‘lcl.1’, and ‘lcl.2’ refer to results on global outliers, and local outliers with respect to clusters 1 and 2

DATA	GBL/LCL	KMEANS-ED	KMEANS-CC	RAND-CC	P1-MEAN	PCAD	RI-DISCORD
gbl	rand	0.00 ± 0.00	0.45 ± 0.44	0.75 ± 0.26	1.00 ± 0.00	1.00 ± 0.00	0.45 ± 0.16
gbl	univ	0.00 ± 0.00	0.50 ± 0.00	0.75 ± 0.26	0.95 ± 0.16	1.00 ± 0.00	0.45 ± 0.16
lcl.1	rand	0.10 ± 0.32	0.33 ± 0.50	0.20 ± 0.42		0.20 ± 0.42	
lcl.1	univ	0.00 ± 0.00	0.00 ± 0.00	0.20 ± 0.42		0.40 ± 0.52	
lcl.2	rand	0.00 ± 0.00	0.60 ± 0.52	0.20 ± 0.42		0.70 ± 0.48	
lcl.2	univ	0.10 ± 0.32	0.10 ± 0.32	0.20 ± 0.42		0.60 ± 0.52	

CEPH and RRL. This demonstrates that even a poorly-formed centroid may be good enough for the task of anomaly detection. The second reason why KMEANS-ED has good results on ogle is that the ogle data set universally-phases well. In Fig. 1, notice that a typical light-curve from each star class has a global maximum. We hypothesize that KMEANS-ED has a better performance on randomly-phased data at higher sample sizes because those centroids tend towards a horizontal line. For global anomaly detection on this synthetically-mixed



ogle data set, a horizontal line is a sufficient model for distinguishing EB from CEPH and RRL!

RI-DISCORD's performance is not a reflection upon its ability to handle unphased data. Its poor overall performance is due to the discord definition. These results demonstrate that the farthest nearest neighbor definition is not sufficient for finding the minority classes in these data sets. The results may improve upon changing the discord definition to the farthest distance to its  $k$ -th nearest neighbor, but one must know how to set  $k$  in advance.

The global anomaly results for KMEANS-CC on ogle also demonstrate that  $k$ -means's centroids may be good enough for anomaly detection. Those results are perfect for the same reasons described for KMEANS-ED. However, for the data sets that do not universally-phase well, its precision results on randomly- and universally-phased data are similarly weak. This is also true for local anomaly results on mallat, nose and landcover. The results for KMEANS-CC and KMEANS-ED show that bad centroids may be good enough for some data sets, but the centroid generation of  $k$ -means is not robust in general. It is certainly not sufficiently robust for local anomaly detection.

RAND-CC has perfect precision on global anomaly detection on the ogle and mallat (its line is superimposed on top of PCAD's and P1-MEANS's in the figures), but performs below PCAD on the landcover and nose data sets for global anomaly detection. It always performs below PCAD for local anomaly detection. Also, RAND-CC always has a higher standard deviation on its results compared to PCAD. RAND-CC's random selection of centroids averts the bad centroid problem of KMEANS-CC and KMEANS-ED, but leads to a higher variation in the quality of anomalies found. Random centroids are clearly inferior to  $k$ -means-generated centroids for local anomaly detection.

P1-MEAN is closest in performance to PCAD. Its global anomaly results are either perfect or nearly perfect on nose, mallat and ogle. However, PCAD has better performance on landcover. The landcover data set is the hardest of the four synthetically-mixed sets. The data have a high signal-to-noise ratio and there is a lot of variance within each class. Under these circumstances, PCAD's multiple centroids model the data better than P1-MEAN's single centroid.

## 8.2 Light-curve data with unknown anomalies

In the next sections we move on to experiments with data sets CEPH, EB, and RRL. Because these data sets contain an unknown number of anomalies, it is not possible to report precision. The reporting of precision would require our domain experts to examine the top  $m$  list of outliers from each experimental iteration, an act which is too time-consuming. Our experts examine a single set of results in Sect. 8.5.

We measure how well PCAD and Protopapas\_n (described in Sect. 7.2) approximate PN-MEANS by measuring the change in rank of PN-MEANS's top  $m$  anomalies. Specifically, we compare the rankings of PN-MEANS's  $m$  most anomalous light-curves to the rankings produced by either PCAD or Protopapas\_n, seeking a minimal change in rank between the two methods. For example, if  $m = 3$  and PN-MEANS and PCAD rank the top three light-curves at 1, 2, and 3, and 1, 6, and 7, respectively, then these light-curves have a rank change of  $|1 - 1| = 0$ ,  $|2 - 6| = 4$ , and  $|3 - 7| = 4$  respectively.

We first show results for the detection of global anomalies on CEPH, EB, and RRL. We experimented with values of  $k$  in [1, 10] and sample sizes [100, 1000] at ten iterations each. We then set PCAD to return a ranked list of 100 light-curves, and average the rankings of the ten iterations with the highest BIC. Figure 10 shows our histograms of rank change that compare PCAD and Protopapas\_n to benchmark PN-MEANS on sample size 500 (chosen

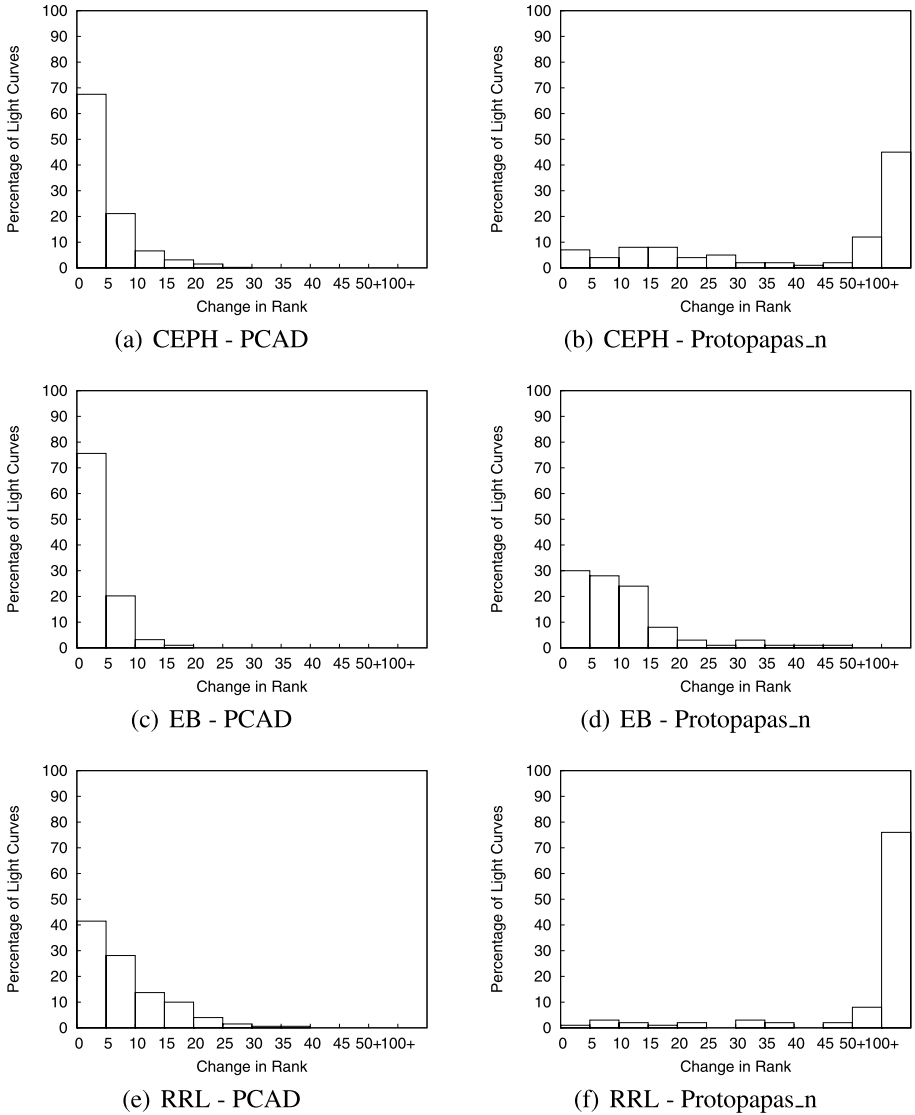


**Fig. 10** Histograms of rank change comparing the rankings of both PCAD and Protopapas\_n to the benchmark PN-MEANS

arbitrarily). In all cases, PCAD’s anomaly rankings are much closer to those of PN-MEANS than Protopapas\_n’s rankings. Thus, PCAD is the better approximation of PN-MEANS. Protopapas\_n fares better on the EB data set because it is a higher variance data set whose outliers are more discernible.

### 8.3 Effect of sample size

We also compare the quality of approximation among PCAD, RAND-CC, and RAND-CC-GAUSS (recall from Sect. 7.2 that RAND-CC and RAND-CC-GAUSS can be considered

SS	PCAD	RND-CC	RND-CC-G
20		6.29 ± 1.67	69.50 ± 76.25
40		4.49 ± 1.12	20.86 ± 16.80
60		4.26 ± 0.57	14.26 ± 10.70
80		3.86 ± 0.51	7.82 ± 2.06
100	4.19 ± 1.86	4.54 ± 0.60	13.68 ± 6.37
200	2.22 ± 1.43	4.22 ± 0.43	8.37 ± 2.17
400	1.97 ± 1.11	4.05 ± 0.19	8.05 ± 0.95
600	1.20 ± 0.45	4.22 ± 0.16	8.82 ± 0.42
800	1.04 ± 0.25	4.22 ± 0.18	10.77 ± 0.72
1000	0.78 ± 0.38	4.27 ± 0.10	14.72 ± 0.51

(a) CEPH

SS	PCAD	RND-CC	RND-CC-G
20		3.72 ± 0.80	8.96 ± 3.83
40		2.90 ± 0.53	8.33 ± 1.74
60		2.82 ± 0.41	7.63 ± 1.88
80		2.44 ± 0.27	6.42 ± 1.15
100	5.37 ± 1.01	2.73 ± 0.55	7.57 ± 2.31
200	4.46 ± 0.73	2.50 ± 0.22	8.04 ± 1.49
400	3.36 ± 1.27	2.28 ± 0.21	7.56 ± 1.22
600	2.35 ± 0.86	2.25 ± 0.17	7.64 ± 0.24
800	1.31 ± 0.35	2.31 ± 0.12	7.96 ± 0.70
1000	1.29 ± 0.58	2.30 ± 0.09	8.34 ± 0.62

(b) EB

SS	PCAD	RND-CC	RND-CC-G
20		7.61 ± 1.17	10.62 ± 4.67
40		7.13 ± 0.85	7.05 ± 2.21
60		6.84 ± 0.66	6.26 ± 2.74
80		6.88 ± 0.53	8.03 ± 2.60
100	3.56 ± 0.75	6.87 ± 0.21	6.61 ± 1.28
200	2.80 ± 0.88	6.73 ± 0.36	5.30 ± 0.67
400	2.07 ± 0.33	6.72 ± 0.21	5.68 ± 0.57
600	1.55 ± 0.27	6.82 ± 0.19	5.65 ± 0.54
800	1.33 ± 0.40	6.78 ± 0.14	5.93 ± 0.63
1000	0.99 ± 0.28	6.81 ± 0.13	5.88 ± 0.59

(c) RRL

**Fig. 11** Comparison of mean rank change of the top 100 light-curves of PCAD, RAND-CC and RAND-CC-GAUSS on CEPH, EB and RRL using varying sample sizes (SS). For PCAD, sample size refers to the size of the data set Pk-means is run on. Pk-means produces no more than ten centroids for outlier score calculation. For RAND-CC and RAND-CC-GAUSS, sample sizes refers to the number of centroids that the outlier scores was calculated with

sampld versions of PN-MEANS). In Fig. 11, we show the effects of sample size on both PCAD, RAND-CC, and RAND-CC-GAUSS. For all methods, it is important to understand how the term sample size is used. For PCAD, a sampling of the data is used by Pk-means to generate a relatively small set of centroids. For both RAND-CC methods, the samplings are used directly as the centroids for comparison. Thus, for the RAND-CC methods, sample size and centroid size can be used interchangeably. For PCAD, sample size and centroid size

are distinct entities. The centroid size of PCAD is chosen by BIC. In our experiments, the number of centroids that maximizes BIC is never more than ten.

We compare PCAD to both RAND-CC methods on a wide range of sample sizes (between 10 and 1000). The purpose of testing on smaller sample sizes is to compare PCAD and the RAND-CC methods when they use a comparable number of centroids. We compare performance at larger sample sizes to test the effect of directly converting the sampling intended for Pk-means into the reference set of centroids used by RAND-CC. Of course, at larger sample sizes, the computational expense of both RAND-CC methods increases, approaching  $O(n^2)$  as the sample size approaches the size of the data set. Thus, it is not desirable for RAND-CC to use too large a sample.

Figure 11 shows average change in rank between each method and PN-MEANS for the top 100 anomalies. For PCAD, the results show that increasing the sample size used by Pk-means improves PCAD's ability to approximate PN-MEANS. At a sample size of 1000, the average rank change of the top 100 anomalies is less than 1.30 for all star classes. Both RAND-CC methods do not approach this level of approximation, even at sample sizes (really, centroid sizes) of 1000. RAND-CC-GAUSS, which differs from RAND-CC in using a Gaussian-weighted outlier scoring function, shows extremely high variability at small sample sizes. This is because Gaussian weighting does not work well with small sample sizes. Another observation is that the average rank change values do not decrease monotonically for RAND-CC-GAUSS, though the trend is generally downward. But despite this downward trend, RAND-CC-GAUSS never outperforms PCAD, even at sample size 1000. This is particularly surprising for the CEPH data set, where 1000 examples is approximately 75% of the data. Independently, we verified that when the sample size approaches the actual size of the data, the rank change does indeed converge to 0 for RAND-CC-GAUSS. So, even with 75% of the data set represented in the sample, the variability of the sample causes RAND-CC-GAUSS to underperform PCAD as an approximation method. Our hypothesis for why both RAND-CC methods underperform is that their outlier score calculations are exposed to the effects of noise in the light-curves and variability in the sample. Meanwhile, PCAD is effective despite using small numbers of centroids because Pk-means is able to effectively mitigate both effects and produce a reliable set of centroids.

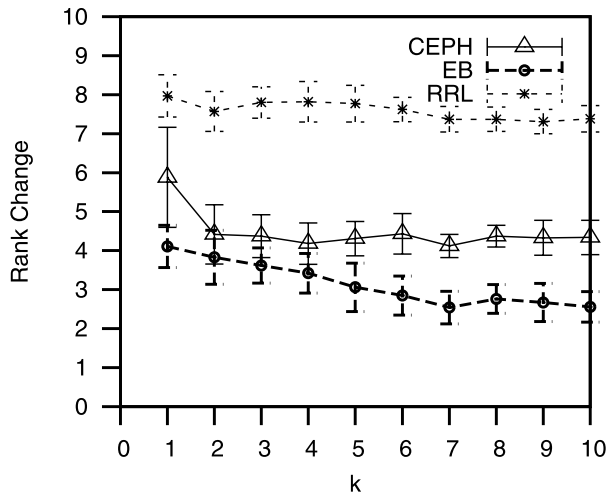
#### 8.4 Effect of parameter $k$

We currently use BIC as a guideline for the selection of  $k$ . Figure 12 shows average change in rank between each PCAD and PN-MEANS for the top 100 global anomalies over increasing values of  $k$ . The results show that a wide range of  $k$  does not greatly impact the rankings. One might conclude from these results that the selection of  $k$  may be trivial, and one can choose  $k = 1$  and reduce the computational cost of Pk-means. However, our earlier experimental results comparing PCAD to P1-MEAN (Fig. 7) justified our multi-centroid approach. Furthermore, a choice of  $k = 1$  eliminates the possibility of finding local anomalies.

#### 8.5 Astrophysicists' review of anomalies

We conclude our experimental section with an analysis of the anomalies output by PCAD by the astrophysicists on our project (Protopapas and Alcock). For the data sets CEPH, EB and RRL, they reviewed PCAD's ten most anomalous light-curves and categorized the anomalies as follows: (a) noisy light-curves with high observational errors, (b) light-curves that were misclassified (e.g., a light-curve in the CEPH data set that was not a Cepheid), and (c) interesting examples worthy of further study. Figures 13 and 14 show some of the

**Fig. 12** Effect of  $k$  on PCAD. The y-axis measures average change in rank from PN-MEAN over PCAD's top 100 anomalies

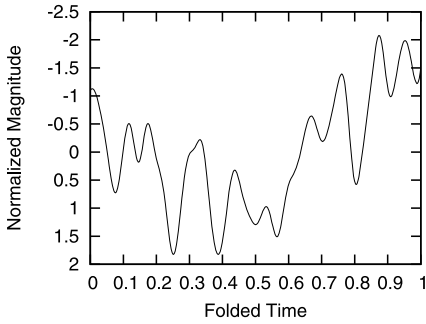


more interesting anomalies. Please note that we show the pre-processed version of each light-curve for clarity's sake, but our astrophysicists had the original folded light-curves as well as other information at their disposal.

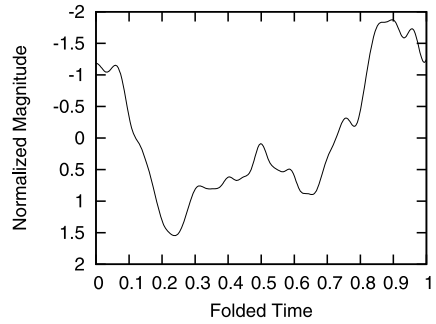
We find that PCAD's top anomalies from the CEPH data set have few true anomalies. The light-curve in Fig. 13(a) is an example of a light-curve that lacks a strong period and has high observational errors. As it stands, its slow rise and fast decline is atypical of Cepheids, but its measurements are too noisy to definitively conclude it is an anomaly. The light-curves in Figs. 13(b), 13(c) and 13(d) exhibit the wrong asymmetry and are most likely incorrectly classified as Cepheids. The light-curve in Fig. 13(e) has a long plateau which is atypical of Cepheid stars, and is most likely not a Cepheid. The light-curve in Fig. 13(f) is interesting. The overall shape, period and color (which are information accessible to the astrophysicists) are consistent with a Cepheid. However, its regularly spaced spikes cannot be dismissed as noise, and may be indicative of an underlying dynamical process. A more careful study of this light-curve is needed to understand its underlying physical process.

PCAD's top EB anomalies all have eccentric orbits, and are justifiably flagged as anomalies. Only the light-curve in Fig. 14(a) is not a typical Eclipsing Binary. There is either a third body present in the system producing a second occultation or some form of atmospheric variation in one of the stars in the system. There also might be a large reflection effect, which occurs when the side of the dimmer star that is facing the Earth is illuminated by the brighter companion star, thus increasing the luminosity of the system (Pollacco and Bell 1993). This light curve also warrants further investigation.

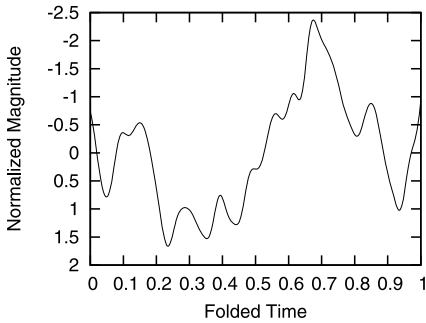
Among the RRL light-curves, PCAD identified two light curves that are most likely misclassified. The light-curve in Fig. 14(b) has a quoted period and amplitude that does not correspond to a typical RR Lyrae. Furthermore, it may not even be a periodic star. The light-curve in Fig. 14(c) does not have a strong signal and has a long plateau which is atypical of RRL. The rest of the anomalies are very faint objects that have the characteristic shape of a RR Lyrae, but a low signal-to-noise ratio that causes them to appear different from the rest of the data set.



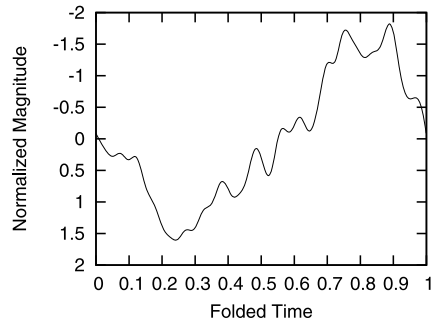
(a) 17.70123 (CEPH)



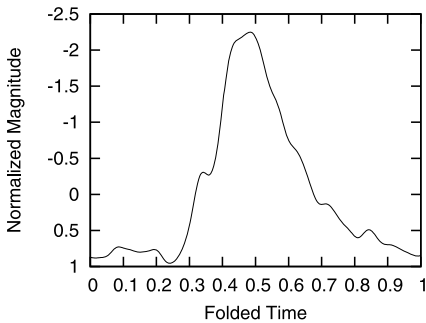
(b) 13.184117 (CEPH)



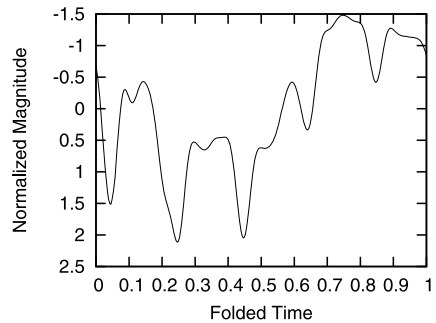
(c) 20.54206 (CEPH)



(d) 13.203944 (CEPH)



(e) 11.331601 (CEPH)



(f) 21.40876 (CEPH)

**Fig. 13** Selected anomalies (light-curve name and class appear below each figure). Note that the pre-processed versions of these light-curves are shown for purposes of clarity

### 9 Conclusion and future work

This paper establishes PCAD as a method that discovers distance-based local and global anomalies on unsynchronized periodic time series data. We use unsupervised learning to generate a set of representative time series centroids from which the anomaly scores are calculated. Our method is able to scale to large data sets through the use of sampling. The online portion of our method is linear in the size of the data.

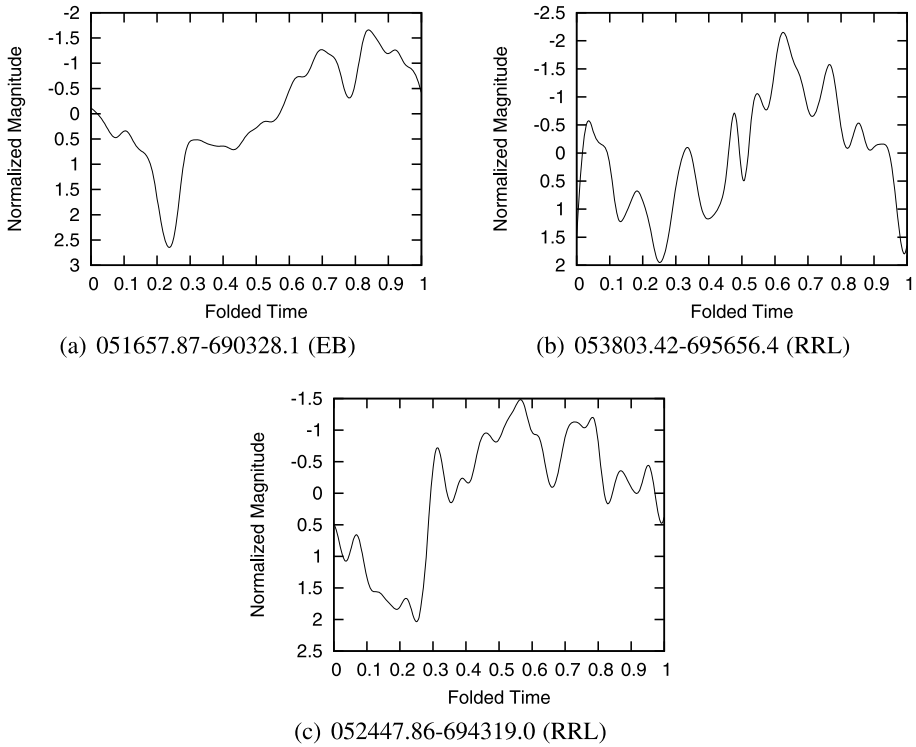


**Fig. 14** Selected anomalies (continued). Note that the pre-processed versions of these light-curves are shown for purposes of clarity

In future work, we wish to develop density-based anomaly scores and ranking methods that are robust to variance within a data set. We also wish to validate our technique on larger amounts of light-curve data. Specifically, our astrophysics collaborators will soon have access to billions of light-curves through the Pan-STARRS survey. This data will be the ultimate test of PCAD's scalability. We also wish to incorporate the observational errors of the light-curves into the PCAD algorithm, in order to fully automate the anomaly detection process.

**Acknowledgements** The authors would like to acknowledge Dr. Anselm Blumer and Dr. Roni Kharon of Tufts University for their helpful guidance and comments. We also acknowledge Dr. Mark Friedl of Boston University for the donation of the landcover data set, and Dr. David Walt and Matthew Aernecke of Tufts University for the donation of the nose data set. This material is based upon work supported by NASA under Grant No. NNX07AV75G, and the NSF under Grant No. IIS0713259.

## References

- Aggarwal, C. C., & Yu, P. S. (2001). Outlier detection for high dimensional data. In *Proceedings of the ACM SIGMOD international conference on data management* (pp. 37–46).
- Angiulli, F., & Pizzuti, C. (2002). Fast outlier detection in high dimensional spaces. In *PKDD'02: Proceedings of the 6th European conference on principles of data mining and knowledge discovery* (pp. 15–26).
- Bar-Joseph, Z., Gerber, G., Gifford, D. K., Jaakkola, T., & Simon, I. (2002). A new approach to analyzing gene expression time series data. In *RECOMB* (pp. 39–48).

- Barnett, V., & Lewis, T. (1994). *Outliers in statistical data*. New York: Wiley.
- Bay, S. D., & Schwabacher, M. (2003). Mining distance-based outliers in near linear time with randomization and a simple pruning rule. In *Proceedings of the ninth international conference on knowledge discovery and data mining* (pp. 29–38).
- Bottou, L., & Bengio, Y. (1995). Convergence properties of the k-means algorithms. In *Advances in neural information processing systems* (pp. 585–592).
- Breunig, M. M., Kriegel, H., Ng, R. T., & Sander, J. (2000). LOF: Identifying density-based local outliers. In *Proceedings of the ACM SIGMOD international conference on management of data* (pp. 93–104).
- Chan, P. K., & Mahoney, M. (2005). Modeling multiple time series for anomaly detection. In *IEEE international conference on data mining* (pp. 90–97).
- Chudova, D., Gaffney, S., Mjolsness, E., & Smyth, P. (2003). Translation-invariant mixture models for curve clustering. In *Proceedings of the 9th ACM SIGKDD international conference on knowledge discovery and data mining* (pp. 79–88).
- Dasgupta, D., & Forrest, S. (1996). Novelty detection in time series data using ideas from immunology. In *Proceedings of the international conference on intelligent systems* (pp. 82–87).
- Dempster, A. P., Laird, N. M., & Rubin, D. B. (1977). Maximum likelihood from incomplete data via the EM algorithm. *Journal of the Royal Statistical Society*, 39, 1–38.
- Gaffney, S., & Smyth, P. (2004). Joint probabilistic curve clustering and alignment. In *Advances in neural information processing systems* (Vol. 17, pp. 473–480). Cambridge: MIT Press.
- Hawkins, D. (1980). *Identification of outliers*. London: Chapman and Hall.
- Hewish, A., Bell, J., Pilkington, P., & Scott, R. (1968). Observations of a rapidly pulsating radio source. *Nature*, 217, 709–710.
- Jagadish, H. V., Koudas, N., & Muthukrishnan, S. (1999). Mining deviants in a time series database. In *Proceedings of the 25th international conference on very large data bases* (pp. 102–113).
- Jin, W., Tung, A. K. H., & Han, J. (2001). Mining top-n local outliers in large databases. In *Proceedings of the seventh ACM SIGKDD international conference on knowledge discovery and data mining* (pp. 293–298).
- Keogh, E., & Folias, T. (2002). The UCR time series data mining archive. <http://www.cs.ucr.edu/~eamonn/TSDMA/index.html>.
- Keogh, E., Lonardi, S., & Chiu, B. Y. (2002). Finding surprising patterns in a time series database in linear time and space. In *Proceedings of the eighth ACM SIGKDD international conference on knowledge discovery and data mining* (pp. 550–556).
- Keogh, E., Lin, J., & Fu, A. (2005). HOT SAX: Efficiently finding the most unusual time series subsequence. In *Proceedings of the fifth IEEE international conference on data mining* (pp. 226–233).
- Klebesadel, R. W., Strong, I. B., & Olson, R. A. (1973). Observations of gamma-ray bursts of cosmic origin. *Astrophysical Journal Letters*, 182, L85+.
- Knorr, E. M., & Ng, R. T. (1998). Algorithms for mining distance-based outliers. In *Proceedings of the 24th international conference on very large databases (VLDB)* (pp. 392–403).
- Kollios, G., Gunopulos, D., Koudas, N., & Berchtold, S. (2003). Efficient biased sampling for approximate clustering and outlier detection in large data sets. *IEEE Transactions on Knowledge and Data Engineering*, 15(5), 1170–1187.
- Lazarevic, A., & Kumar, V. (2005). Feature Bagging for Outlier Detection. In *Proceedings of the eleventh ACM SIGKDD international conference on knowledge discovery and data mining* (pp. 157–166).
- Lin, J., Keogh, E., Lonardi, S., & Chiu, B. (2003). A symbolic representation of time series, with implications for streaming algorithms. In *Proceedings of the 8th ACM SIGMOD workshop on research issues in data mining and knowledge discovery*.
- Listgarten, J., Neal, R. M., Roweis, S. T., Puckrin, R., & Cutler, S. (2006). Bayesian detection of infrequent differences in sets of time series with shared structure. In *Advances in neural information processing systems 19*.
- Ma, J., & Perkins, S. (2003). Online novelty detection on temporal sequences. In *Proceedings of the ninth ACM SIGKDD international conference on knowledge discovery and data mining* (pp. 613–618).
- Mahoney, M., & Chan, P. K. (2005). Trajectory boundary modeling of time series for anomaly detection. In *Computer Science Dept. Technical Report CS-2005-08*.
- Mallat, S. (1998). *A wavelet tour of signal processing*. San Diego: Academic Press.
- Pelleg, D., & Moore, A. (2000). X-means: Extending K-means with efficient estimation of the number of clusters. In *Proceedings of the 17th international conference on machine learning* (pp. 727–734).
- Petit, M. (1987). *Variable stars*. New York: Wiley.
- Pollacco, D. L., & Bell, S. A. (1993). New light on UU Sagittae. *Monthly Notices of the Royal Astronomical Society*, 262, 377–391.
- Protopapas, P., Giammarco, J. M., Faccioli, L., Struble, M. F., Dave, R., & Alcock, C. (2006). Finding outlier light-curves in catalogs of periodic variable stars. *Monthly Notices of the Royal Astronomical Society*, 369, 677–696.



- Ramaswamy, S., Rastogi, R., & Shim, K. (2000). Efficient algorithms for mining outliers from large data sets. In *SIGMOD'00: Proceedings of the 2000 ACM SIGMOD international conference on management of data* (pp. 427–438).
- Ren, D., Wang, B., & Perrizo, W. (2004). RDF: A density-based outlier detection method using vertical data representation. In *Proceedings of the fourth IEEE international conference on data mining* (pp. 503–506).
- Richter, G., Wenzel, W., & Hoffmeister, C. (1985). *Variable stars*. Berlin: Springer.
- Salvador, S., Chan, P., & Brodie, J. (2004). Learning states and rules for time series anomaly detection. In *Proceedings of the seventeenth international Florida artificial intelligence research society conference*.
- Samus', N. N., Goranskii, V. P., Durlевич, O. V., Zharova, A. V., Kazarovets, E. V., Kireeva, N. N., Pastukhova, E. N., Williams, D. B., & Hazen, M. L. (2003). An electronic version of the second volume of the general catalogue of variable stars with improved coordinates. *Astronomy Letters*, 29(7), 468–479.
- Schmidt, M. (1963). 3c 273: A star-like object with large red-shift. *Nature*, 197, 1040.
- Shahabi, C., Tian, X., & Zhao, W. (2000). TSA-tree: A wavelet-based approach to improve the efficiency of multi-level surprise and trend queries on time-series data. In *Statistical and scientific database management* (pp. 55–68).
- Sterken, C., & Jaschek, C. (1996). *Light curves of variable stars: a pictorial atlas*. Cambridge: Cambridge University Press.
- Udalski, A., Szymanski, M., Kubiak, M., Pietrzynski, G., Wozniak, P., & Zebrun, Z. (1997). Optical gravitational lensing experiment. photometry of the macho-smc-1 microlensing candidate. *Acta Astronomica*, 47(431).
- Wei, L., Kumar, N., Lolla, V., Keogh, E., Lonardi, S., & Ratanamahatana, C. (2005). Assumption-free anomaly detection in time series. In *SSDBM'2005: Proceedings of the 17th international conference on scientific and statistical database management* (pp. 237–240).
- Wei, L., Keogh, E., & Xi, X. (2006). SAXually explicit images: Finding unusual shapes. In *Proceedings of the sixth IEEE international conference on data mining* (pp. 711–720).
- Wu, M., & Jermaine, C. (2006). Outlier detection by sampling with accuracy guarantees. In *Proceedings of the 12th ACM SIGKDD international conference on knowledge discovery and data mining* (pp. 767–772).
- Yang, J., Wang, W., & Yu, P. S. (2001). Infominer: Mining surprising periodic patterns. In *Proceedings of the seventh ACM SIGKDD international conference on knowledge discovery and data mining* (pp. 395–400).
- Yang, J., Wang, W., & Yu, P. S. (2004). Mining surprising periodic patterns. *Data Mining and Knowledge Discovery*, 9, 189–216.
- Yu, D., Sheikholeslami, G., & Zhang, A. (2004). FindOut: Finding outliers in very large datasets. *Knowledge and Information Systems*, 4(4), 387–412.